Article

The DAV132 colon-targeted adsorbent does not interfere with plasma concentrations of antibiotics but prevents antibiotic-related dysbiosis: a randomized phase I trial in healthy volunteers

A list of authors and their affiliations appears at the end of the paper

The deleterious impact of antibiotics (ATB) on the microbiome negatively influences immune checkpoint inhibitors (ICI) response in patients with cancer. We conducted a randomized phase I study (EudraCT:2019-A00240-57) with 148 healthy volunteers (HV) to test two doses of DAV132, a colon-targeted adsorbent, alongside intravenous ceftazidime-avibactam (CZA), piperacillin-tazobactam (PTZ) or ceftriaxone (CRO) and a group without ATB. The primary objective of the study was to assess the effect of DAV132 on ATB plasma concentrations and both doses of DAV132 did not alter ATB levels. Secondary objectives included safety, darkening of the feces, and fecal ATB concentrations. DAV132 was well tolerated, with no severe toxicity and similar darkening at both DAV132 doses. DAV132 led to significant decrease in CZA or PTZ feces concentration. When co-administered with CZA or PTZ, DAV132 preserved microbiome diversity, accelerated recovery to baseline composition and protected key commensals. Fecal microbiota transplantation (FMT) in pre-clinical cancer models in female mice from HV treated with CZA or PTZ alone inhibited anti−PD-1 response, while transplanted samples from HV treated with ATB + DAV132 circumvented resistance to anti−PD-1. This effect was linked to activated CD8^{+} T cell populations in the tumor microenvironment. DAV132 represents a promising strategy for overcoming ATB-related dysbiosis and further studies are warranted to evaluate its efficacy in cancer patients.

Despite the approval of immune checkpoint inhibitors (ICI) in various cancers and recently in the neoadjuvant settings, strategies to decrease resistance to ICI represent an unmet medical need[1,2]. Over the past decade, studies unravelling the cancer-immunity dialogue in the setting of ICI have determined that resistance is profoundly influenced by gut microbiota[3–8]. Several microbiota profiling studies conducted in patients with non-small cell lung cancer (NSCLC), melanoma, or renal

cell carcinoma (RCC) revealed compelling evidence that specific bacteria such as *Akkermansia muciniphila, Ruminococcus,* and *Eubacterium* were associated with recruitment of intratumor CD8^{+} T cells, interferon gamma (INFγ) signalling pathway, and correlated with beneficial ICI response[9–12]. Moreover, transplantation of patients' feces to germ-free mice recapitulated patient outcomes, providing further evidence of the relationship between microbiota composition and

✉ e-mail: Bertrand.routy@umontreal.ca

response to ICI[9,13,14]. Several strategies to modify the microbiota composition including encouraging results from fecal microbiota transplantation (FMT) trials are currently being explored as novel therapeutic interventions to improve ICI response[15–18]. The pivotal evidence supporting the key role of the microbiota in ICI was gathered from antibiotic (ATB)-treated mice, where altering the microbiota by ATB inhibited responses to programmed cell death protein 1 (PD-1) blockers used alone or in combination with a cytotoxic T-lymphocyte associated protein 4 (CTLA-4) inhibitor[9,19]. These observations led to retrospective and prospective studies in several cohorts of cancer patients amenable to ICI, confirming that ATB blunted the efficacy of ICI[20–22]. This observation was validated in a meta-analysis of 105 studies across 46,000 patients with cancer amenable to immunotherapy, demonstrating that ATB use six weeks before ICI initiation was associated with a shorter overall survival[8]. Subsequent studies have characterized the effect of ATB on the taxonomic composition of feces from patients with RCC and NSCLC. At baseline, patients on ATB had lower microbiota diversity and an over-representation of *Hungatella hathewayi* and *Akkermansia muciniphila* beyond the beneficial threshold (77th percentile)[10,13]. Conversely, ATB-naïve patients had an enrichment of *Ruminococcus* and *Agathobacter*[23,24]. These results characterized the deviated repertoire of the intestinal ecosystem post-ATB, referred to as ATB-related dysbiosis, and its impact on ICI outcomes, leading to judicious prescription of ATB in general oncology practice[21]. Clinical studies showed that probiotics post-ATB or prior to ICI failed to restore microbiota composition and decreased ICI efficacy[11,25]. Currently, there is no effective approach to overcome the deleterious impact of ATB on microbiota composition. A strategy to overcome ATB-related dysbiosis is urgently needed given the frequency with which ATB are prescribed in cancer patients on ICI.

Oral ATB adsorbent DAV132 is composed of activated charcoal beads coated with a layer of pH-sensitive enteric polymer ensuring its targeted delivery to the terminal ileum and cecum[26]. Administration of DAV132, together with oral amoxicillin or moxifloxacin in healthy participants, significantly reduces fecal concentrations of the ATB while preserving their pharmacokinetic properties[26,27]. Moreover, in hamster models, DAV132 decreases mortality from *Clostridium difficile* colitis induced by fluoroquinolones and clindamycin[28–30]. Based on these findings, we hypothesized that co-administration of DAV132 with ATB would prevent ATB-related dysbiosis. Here we tested this hypothesis in a prospective longitudinal randomized trial conducted in healthy volunteers (HV; $N = 148$) who were randomized to treatment with ceftazidime-avibactam (CZA) or piperacillin-tazobactam (PTZ) or with ceftriaxone (CRO), with two different doses or without DAV132 as a comparator. Primary and secondary objectives were met for PTZ and CZA.

Here, we show, using metagenomics profiling coupled with bacterial probe set qPCR, that for CZA and PTZ, DAV132 partially protects microbiome diversity and composition, and maintains several bacterial taxa associated with ICI response. Subsequently, using avatar murine models, we demonstrate that protection of DAV132 against ATB-related dysbiosis is adequate to maintain the response to αPD-1.

Results

Characteristics of healthy volunteers

HV were randomly assigned to broad β-lactam with a β-lactamase inhibitor (PTZ), or a third-generation cephalosporin combined with another β-lactam β-lactamase inhibitor (CZA) or third-generation cephalosporin CRO or no ATB[31,32] (Fig. 1A). HV received five days of intravenous (IV) ATB alone or in combination with either 2 doses of DAV132 orally 7.5 g (po) 3 times per day (tid) or 12 g po tid administered for 7 days. Among the 148 HV randomized (three HV withdrew their consent), then from the 145 HV that started the treatment 2 HV were excluded for non-compliance (not related to toxicity) and 1 HV in

the PTZ alone group was excluded by the investigator as the volunteer wanted to stop its participation (Supplementary Fig. 1A). Because these HV took at least 1 dose of DAV132, they were included in the adverse events (AE) analysis but excluded from the pharmacokinetic and microbiome profiling as these latter metrics could not be measured across all timepoints (Supplementary Fig. 1). Among the 142 HV that completed the study, there were (27, 28 and 25%) men in the no DAV groups, DAV132 7.5 g and DAV132 12 g. Median age was 36, 38 and 36-year-old, respectively. The twelve treatment groups were well balanced for age, sex, and body mass index (Supplementary Table 1).

### Primary objective of plasma concentrations of antibiotics in healthy volunteers

To investigate whether DAV132 interfered with the therapeutic index of ATB, systemic plasma pharmacokinetics of CZA, PTZ, CRO, and their respective β-lactamase inhibitors avibactam and tazobactam were measured after injection on Day (D) 5. Plasma concentrations of all ATB and their respective β-lactamase inhibitors were not significantly decreased in the blood of HV when co-administered with both doses of DAV132 (Fig. 1B and Supplementary Fig. 1B).

Second endpoint of safety of DAV132 and darkening of the feces in healthy volunteers

101 (69.7%) HV experienced at least one AE. 68 (70.1%) HV who received DAV132 alone at 7.5 g or at 12 g (DAV132-CTRL) or with an ATB (CZA + DAV132, PTZ + DAV132 or CRO + DAV132) experienced at least one AE, while 33 (68.8%) HV who did not receive DAV132 (i.e., CZA alone, PTZ alone, CRO alone or CTRL alone) experienced at least one AE ($p = 0.87$; Supplementary Table 2). AEs were mild or moderate in intensity; none were severe[33]. All events resolved spontaneously without the need for treatment. The most common AEs observed were gastrointestinal in nature; and there was no difference in AE between DAV132 either dose compared to no DAV132 ($p = 0.89$). Of note one HV in the CRO + DAV 7.5 g group passed away on D25. This AE was declared not related to either ATB or DAV132 by the Investigator. With respect to fecal darkening, there was no difference between the two DAV132 doses regarding the onset of change in feces color (DAV132 7.5 g: 2.0 ± 0.6; DAV132 12 g (2.1 ± 0.6); $p = 0.58$; mean ± SD) and the return to normal (DAV132 7.5 g: 7.0 ± 4.0; DAV132 12 g: 6.5 ± 4.0; $p = 0.49$; mean ± SD) (Supplementary Fig. 1C).

Secondary objective of fecal ATB concentration post DAV132

Measurement of ATB concentrations in fecal samples obtained at different timepoints revealed that in the ATB-alone groups, fecal levels of Ceftavidime and Piperacillin reached levels up to 100 mg/kg feces at D4 and remained detectable at D8 (Fig. 1C). However, in the HV receiving ATB + DAV132, fecal ATB concentrations were significantly reduced to almost undetectable levels regardless of the doses, ($\text{AUC}_{\text{D1-D9}}$: ATB vs. ATB + DAV132 12 g, $p < 0.0001$ and ATB vs. ATB + DAV132 7.5 g $p < 0.002$ and $p < 0.01$ for both Ceftavidime and Piperacillin respectively). Interestingly, DAV132 at the higher dose of 12 g had a slightly superior effect compared to the lower dose. Fecal levels of the β-lactamase inhibitors avibactam and tazobactam were considerably lower than their associated ATBs (< 10 mg/kg); the level of fecal avibactam was somewhat reduced by DAV132, while its effect on tazobactam was more pronounced, as the latter was almost undetectable at the higher dose of 12 g DAV132 (Supplementary Fig. 1D). These findings demonstrated that DAV132, especially at the higher dose, was able to effectively decrease levels of Ceftavidime and Piperacillin in the colon without impacting systemic concentrations. With respect to CRO, the levels of fecal ATB were inferior to 4 mg/kg in 11 HV and reached 800 mg/kg in only one HV (Supplementary Fig. 1D). In order to understand this discrepancy, we measured the level of β-lactamase activity in the corresponding fecal samples. All HV beside the one with
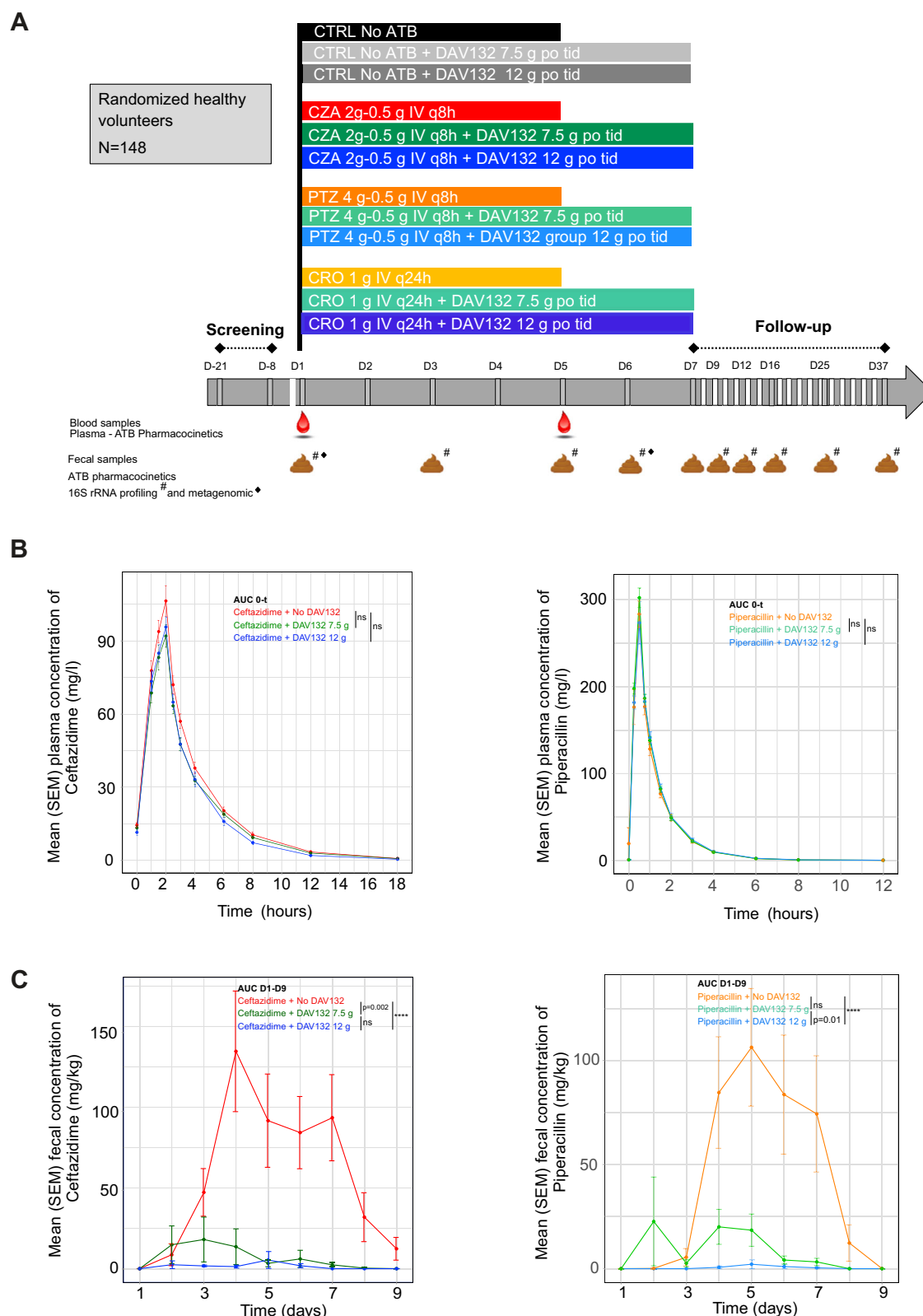
high level of CRO had detectable β-lactamase activity, explaining the low fecal level of CRO (Supplementary Fig. 1E). As anticipated, in absence of CRO in the fecal concentration, the microbiome alpha diversity (α-diversity) was not significantly altered (Supplementary Fig. 1F). Therefore, host β-lactamase represents one way to overcome ATB-related dysbiosis for HV with CRO[34] and in this context, we subsequently excluded these HV from the analysis.

Impact of high DAV132 dose on microbiota diversity of healthy volunteers

Based on the pharmacokinetic results of both DAV132 doses in CZA and PTZ, and without any additional AE, we decided to focus our investigations on the impact of DAV132 on the microbiome at the higher dose. 16S ribosomal RNA (rRNA) gene sequencing from the feces of HV showed that treatment with CZA and PTZ alone triggered

Fig. 1 | Clinical trial design and pharmacokinetics of antibiotics in the plasma and feces of healthy volunteers (HV). A Prospective randomized trial design of 148 HV that included in one of the 12 groups: no ATB control (CTRL) without and with DAV132 alone, CZA or PTZ or CRO alone, or CZA or PTZ or CRO in combination with DAV132. ATB were delivered intravenously for 5 days, while DAV132 was administered orally at two doses either 7.5 g po tid or 12 g po tid for 7 days. **B** Mean plasma concentration (mg/L) of ceftazidime (left panel) and piperacillin (right panel) measured over 18 h after D5. τ was defined as the time interval between two administrations (8 h for PTZ, 8 h for CZA, 24 h for CRO). **C** Mean fecal concentration (mg/kg) of ceftazidime (left panel) and piperacillin (right panel) measured over 9 days. AUC of antibiotics concentrations were compared between arms using an ANOVA, followed by pairwise comparisons with a Tukey's adjustment, $n = 11$–13 HV per group. ATB antibiotic, AUC area under the curve, CZA ceftazidime-avibactam, D day, po orally, PTZ piperacillin-tazobactam, CRO ceftriaxone, q8h every 8 h, q24hr every 24 hour, rRNA ribosomal RNA, tid three times a day, hashtag 16S rRNA sequencing performed, black diamond, metagenomic sequencing performed. (ns non-significant, ****$p < 0.0001$). Source data are provided as a Source Data file.

profound fecal bacteria depletion with a nadir at D6 compared to both control or DAV132 co-administered with ATB groups, as measured by the Shannon α-diversity Index, respectively (CTRL group: mean = −0.378 ± 0.201 (SEM); CZA: mean = −2.4 ± 0.465 (SEM); CZA + DAV132 12 g: mean −0.671 ± 0.253; $p < 0.0001$) and (Ctrl group: mean = −0.378 ± 0.201 (SEM); PTZ: mean = −1.91 ± 0.461 (SEM); DAV132 12 g: mean −0.578 ± 0.271; $p = 0.008$) (Fig. 2A). Thereafter, microbiome diversity increased; however, it did not recover to baseline until more than 30 days after cessation of the ATB treatment (D37). Moreover, when we calculated the change from baseline Shannon Index to D16 (AUC$_{D1-D16}$), there was a significant difference between ATB and control groups. Conversely, DAV132 co-administered with ATB prevented the loss of α-diversity compared to the control group AUC$_{D1-D16}$ for both CZA (CTRL group: mean = 6.1 ± 1.3 (SEM); CZA + DAV132 12 g: mean 7.1 ± 1.0; $p = 0.89$) and PTZ (CTRL group: mean = 6.1 ± 1.3 (SEM); PTZ + DAV132 12 g: mean 8.7 ± 1.3; $p = 0.46$) (Fig. 2A). Of note, the administration of DAV132 alone had no significant impact on microbiota α-diversity compared to the CTRL (without ATB) (Supplementary Fig. 1G).

To assess the impact of DAV132 on the global composition of the microbiota community compared to the ATB-alone and control groups, β-diversity analysis based on the Bray–Curtis dissimilarity index was performed at baseline (D1), after the end of ATB treatment (D6), and during long-term follow-up (D16, D25, and D37; Fig. 2B). At baseline, there was a clustering of all HV regardless of the treatment (CZA: $p = 0.211$; PTZ: $p = 0.393$). At D6, we observed a significant shift in microbiota composition in both ATB and ATB + DAV132 groups compared to the control group (CZA vs. CTRL: $p = 0.001$; CZA + DAV132 vs. CTRL: $p = 0.001$; PTZ vs. CTRL: $p = 0.002$; PTZ + DAV132 vs. CTRL: $p = 0.002$), as well as between the ATB and ATB + DAV132 groups (CZA: $p = 0.001$; PTZ: $p = 0.003$). The microbiota composition of HV in the CZA + DAV132 group reached the composition observed in the control group at D25, while the PTZ + DAV132 group reached this point at D16. Conversely, the differences observed in the CZA ($p = 0.006$) and PTZ ($p = 0.06$) groups compared to control were maintained at 37 days (Fig. 2B). To evaluate the amplitude of β-diversity variations between each group, we measured the Bray–Curtis dissimilarity between ATB or ATB + DAV132 groups versus the control group. As early as D6, the ATB + DAV132 groups presented a significantly lower dissimilarity distance compared with the control groups than the ATB groups (CZA: $p = 0.013$; PTZ: $p = 0.004$) (Fig. 2C). This difference was maintained until D16 for CZA ($p = 0.043$) and D25 for PTZ ($p = 0.005$). Taken together, these results showed that the use of ATB was associated with profound dysbiosis in terms of bacterial diversity and global composition, and that DAV132 exerted partial yet significant protection of the intestinal microbiota.

Protective effect of DAV132 on microbiota taxa of healthy volunteers

To examine the effect of ATB treatments and DAV132 co-administration at the level of individual taxa, we presented 16S rRNA sequencing relative abundance of the most prevalent microbiota community members in the form of heatmaps.
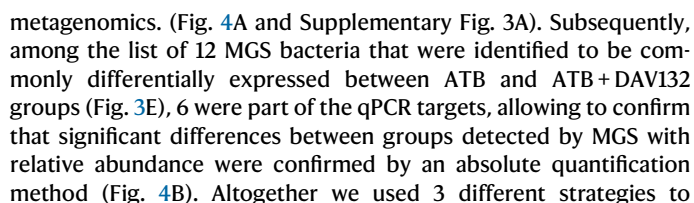
We demonstrated that DAV132 given alone had little impact on the microbiota compared with the untreated control group (Supplementary Fig. 2A). Heatmap representation of the microbiota from the CZA and CZA + DAV132 groups showed that DAV132 was able to maintain a large portion of the microbial taxa that are no longer detected at D6 with CZA treatment (Fig. 3A). Because of this protection at D6, DAV132 was associated with a better overall recovery at D16 compared to baseline. Similarly, heatmaps of the PTZ and PTZ + DAV132 groups also confirmed that DAV132 protected a large part of the microbiota community during ATB treatment, and that their microbial composition observed at D16 are therefore closer to those at baseline in HV treated with PTZ + DAV132 than with PTZ alone (Supplementary Fig. 2B). To further determine which bacterial species were differentially abundant between the ATB and ATB + DAV132 groups, we performed shotgun metagenomics on the feces of HV from these four treatment groups at D1 and D6. Using pairwise comparisons with a Wilcoxon test corrected for parallel multitesting, no baseline (D1) differences were observed between the CZA and CZA + DAV132 groups, or between the PTZ and PTZ + DAV132 groups (Fig. 3B, Supplementary Fig. 2C). At D6, 50 MetaGenomic Species (MGS) were significantly enriched in the CZA + DAV132 group compared with the CZA group. These included *Faecalibacterium* species (e.g., *prausnitzii*), several *Alistipes* members (e.g., *putredinis, shahii, finegoldii*), *Blautia obeum, Eubacterium ramulus, E. boltea*, and *Ruthenibacterium lactatiformans* (Fig. 3C). Conversely, only three bacterial taxa were increased in the CZA group, namely *Enterococcus faecium*, a member of the *Clostridia* class, and *Faecalibacterium longum*. At D6, 41 bacterial metagenomics sequencing, including *Dorea, Ruminococcus sp. AM42-11, Blautia obeum*, several Eubacteriales members, and *Ruthenibacterium lactatiformans*, were over-represented in the PTZ + DAV132 group while none were significantly enriched in the PTZ group (Fig. 3D).

To elucidate which bacteria were commonly preserved by DAV132, we determined the commonly differentially expressed bacteria between the ATB and ATB + DAV132 groups. Eighteen MGS were commonly increased in the CZA + DAV132 and PTZ + DAV132 groups among which 12 were identified at the genus and/or species level (Fig. 3E). These included *Alistipes shahii, Ruthenibacterium lactatiformans, Blautia obeum* and *Intestinimonas butyriciproducens*.

Validation of the protective role of DAV132 on the microbiome composition using qPCR

To further strengthen the results generated by 16S rRNA coupled with metagenomics sequencing, we conducted a qPCR-based assay on a chip using 107 different bacteria probes (BIO-ME) on 79 samples from the 4 different groups. Similarly, to the other sequencing strategies, when we generated heatmaps with representation of the entire bacteria tested on the qPCR panel, we observed that compared to ATB group (CZA or PTZ) alone in the CZA or PTZ in combination with DAV132 was able to protect several gut bacteria (Supplementary Fig. 2D, E). Next, to confirm the concordance between the metagenomics and qPCR results, we selected 84 common bacteria present in both modalities and represented D1, D6 and D16 in heatmap (Fig. 4A and Supplementary Fig. 3A). Next, we used the Kendall score to estimate the level of correlation between qPCR and metagenomics, and a high Kendall score was obtained for most bacteria. Zero Kendall scores were obtained only for *Bifidobacterium breve* and *Solobacterium morel* although both were consistently not detected by

metagenomics. (Fig. 4A and Supplementary Fig. 3A). Subsequently, among the list of 12 MGS bacteria that were identified to be commonly differentially expressed between ATB and ATB + DAV132 groups (Fig. 3E), 6 were part of the qPCR targets, allowing to confirm that significant differences between groups detected by MGS with relative abundance were confirmed by an absolute quantification method (Fig. 4B). Altogether we used 3 different strategies to

demonstrate that DAV132 was able to preserve several bacteria despite two broad spectrum ATB.

Protective role of DAV132 following fecal microbiota transfer in avatar mice

To establish a cause-and-effect relationship between distinct commensals protected by DAV132 post-ATB treatment and the anti-cancer

Fig. 2 | Impact of DAV132 12 g on the gut microbiome in healthy volunteers (HV). A 16S rRNA microbiota profiling: mean change in α-diversity from baseline as measured by the Shannon Index in HV treated in CTRL, CZA, and CZA + DAV132 (left panel), and CTRL, PTZ, and PTZ + DAV132 (right panel) groups. AUC of change from baseline of the Shannon index until D16 were compared between arms using an ANOVA, followed by pairwise comparisons with a Tukey's adjustment. **B** Bray–Curtis representation for beta diversity (β-diversity) between HV treated with CTRL, CZA, and CZA + DAV132 (upper panel) at D1, D6, D25, and D37, and in CTRL, PTZ, and PTZ + DAV132 (lower panel) at D1, D6, D16, and D37. Global and pairwise PERMANOVA were used to compare differences in β-diversity between groups. **C** Bray–Curtis distance measure between control and CZA or CZA + DAV132 at D1, D6, and D16 (upper panel) and between control and PTZ or PTZ + DAV132 (lower panel) at D1, D6, and D25. AUC area under the curve, CTRL control, CZA ceftazidime-avibactam, D day, ns not significant, PTZ piperacillin-tazobactam, DAV132, DAV132 12 g po tid. (ns non-significant, ****$p < 0.0001$). Source data are provided as a Source Data file.

PD-1 response, we recolonized C57BL/6 germ-free or ATB-treated mice by fecal microbiota transplantation (FMT) using fecal samples collected from HV in our clinical trial. As previously published, 2 weeks after FMT, MCA-205 tumor cells were inoculated, and anti-PD-1 (αPD-1) or Iso-control were injected intraperitoneally every 4 days (Fig. 5A)[9,15]. First, FMT was performed on germ-free mice housed in distinct cages using feces collected before treatment initiation (D1) from three separate HV who received CZA (HV 1, 2, and 3) and from three separated HV who received CZA + DAV132 (HV 4, 5, and 6). All fecal samples collected at baseline conferred sensitivity to αPD-1 (Fig. 5B, C and Supplementary Fig. 3B). Second, we performed FMT using fecal samples obtained at D6 from the same HV. FMT from CZA HV (HV 1, 2, and 3) inhibited αPD-1 efficacy, while αPD-1 activity was maintained in mice transplanted with feces from HV who had received DAV132 together with CZA (HV 4, 5, and 6) (Fig. 5B, C and Supplementary Fig. 3B). Experiments were repeated in ATB-treated mice and similarly to the findings from germ-free mice, we only observed αPD-1 anti-tumor activity in mice that had been transplanted with D6 fecal samples from HV who received CZA + DAV132 (Fig. 5D, E and Supplementary Fig. 3C). The finding that the microbiota of CZA HV, but not of CZA + DAV132 HV, at D6 inhibited αPD-1 response was corroborated in a second murine tumor model using melanoma B16-OVA tumor cells (Fig. 5F and Supplementary Fig. 3D).

To validate the biological importance of bacteria protected by DAV132, we also recolonized ATB-treated mice with feces from three PTZ HV (HV 7, 8, and 9) and from three PTZ + DAV132 HV (HV 10, 11, and 12) at D1 and D6. αPD-1 responses were observed in mice transplanted with D1 fecal samples from all six HV. Mice recolonized with D6 fecal samples from PTZ + DAV132 HV, but not PTZ HV, maintained anti–PD-l responsiveness (Fig. 5G and Supplementary Fig. 3E). Taken together, these results suggest that DAV132 can sufficiently maintain the microbiome composition to preserve αPD-1 response. Flow cytometry analysis of tumor infiltrating lymphocytes was performed to assess immune differences between mice receiving FMT from CZA HV versus CZA + DAV132 HV. This analysis revealed an accumulation of CD8⁺ T cells and an increase in the ratio of CD8/Treg (CD4⁺FoxP3⁺ T cells) in both murine tumor models (MCA-205 and B16) recolonized with FMT from HV who had received DAV132 (Fig. 6A and Supplementary Fig. 4A, B). Next, we explored sub-populations of CD8⁺ T cells using staining for 13 immune checkpoints. Uniform Manifold Approximation and Projection (UMAP) dimensional reduction and unsupervised clustering revealed three distinct activated populations significantly increased in the tumor microenvironment of mice that received FMT from DAV132 samples, namely population 8 (CD8⁺T cells: CD45RB⁺, GITR⁺, ICOS⁺, 4-1BB⁺), population 11 (CD8⁺T cells: GITR⁺, ICOS⁺), and population 18 (CD8⁺T cells: CD45RB⁺, GITR⁺, 4-1BB⁺) (Fig. 6B, C and Supplementary Fig. 4C). Subsequently, to support this observation, tumor transcriptome profiling RNA-seq of the bulk murine tumor showed that compared to the three other groups refractory to αPD-1, DAV132 group treated with αPD-1 had unique transcriptome profile (Fig. 6D). Then using ImmuCellAI-mouse program to estimate the immune cells obtained from RNAseq total CD8⁺ T cells as well as CD8⁺ T central memory (TCM CD8⁺ T cells) were increased in group treated with DAV132 and αPD-1 (Fig. 6E and Supplementary Fig. 4D). To further characterize CD8⁺ T cells, RNAseq on cell-sorted CD8⁺ T cells revealed

that mice in the DAV132 + αPD-1 group had a unique signature (Fig. 6F) with a downregulation of inflammatory pathways including IL-6 and reactive oxygen species (ROS) (Supplementary Fig. 4E). Lastly, and consistent with the cytotoxic CD8⁺ T cells in the TILs we observed an upregulation of *ifng* and the ratio *ifng/il-10* in the mesenteric and tumor draining lymph nodes (Fig. 6G). Altogether, these results suggest an association between the microbiome of HV on DAV132 and more cytotoxic CD8⁺ T cells in TILs post αPD-1 treatment.

Murine 16S rRNA gene sequencing confirms that engraftment from HV correlates with αPD-1 outcome

To determine that the bacterial engraftment correlated with the microbiota of HV FMT donors, we compared the Shannon α-diversity index of individual HV to that of feces collected from the recipient germ-free mice. We observed a positive correlation between the α-diversity of HV and the diversity of engrafted bacteria in recipient mice (Supplementary Fig. 5A). There was no difference in α-diversity between mice that received FMT using fecal samples collected at D1 from CZA HV versus CZA + DAV132 HV (Supplementary Fig. 5B). Conversely, mice recolonized with FMT using samples collected at D6 from CZA HV had a significant lower α-diversity than those recolonized from CZA + DAV132 HV samples ($p = 0.005$). Of note, for each FMT the impact of treatment (Iso-PD-1 vs αPD-1) was not significant (Supplementary Fig. 5C).

To further visualize the difference in HV microbiota and engraftment in mice, we used a histogram representing the microbiota composition at the family level of HV (D1 and D6) and subsequent engraftment in mice (Fig. 7A). Furthermore, a principal coordinates analysis using all murine fecal samples showed that mice that received FMT from CZA HV at D6 cluster to the left of the principal axis. In contrast, mice that received FMT from CZA + DAV132 HV at D1 or D6, and from CZA HV at D1, which are associated with an αPD-1 response, cluster to the right of the principal axis ($p = 0.001$) (Fig. 7B). Finally, a differential analysis demonstrated that mice receiving FMT from HV prior to the initiation of ATB (D1) had an abundance of *Alistipes, Ruminococcaceae, Christensenellaceae R-7 group*, and that this microbiota was preserved in mice receiving FMT from HV who received CZA + DAV132, but not CZA alone at D6 (Fig. 7C). Altogether these preclinical models confirmed that the composition of the microbiota in the mice correlated with the HV microbiota and that enough immunogenic bacteria were preserved in HV with DAV132 to maintain strong αPD-1 activity.

Discussion

Use of ATB represents a negative prognostic factor for patients amenable to ICI but there are currently no evidence-based strategies to overcome ATB-related dysbiosis[7]. We reported the first-in-human study of concomitant use of the colon-targeted adsorbent, DAV132, with two distinct broad-spectrum ATB with β-lactamase inhibitor combinations frequently used in the treatment of sepsis in oncology patients[31,35]. Our clinical and translational research represents one potential safe strategy to successfully overcome the deleterious effects of ATB-related. We demonstrated that both DAV132 dosing significantly reduced CZA and PTZ concentration in the colon, but not in the plasma, of HV. Furthermore, we showed that DAV132 at 12 g tid
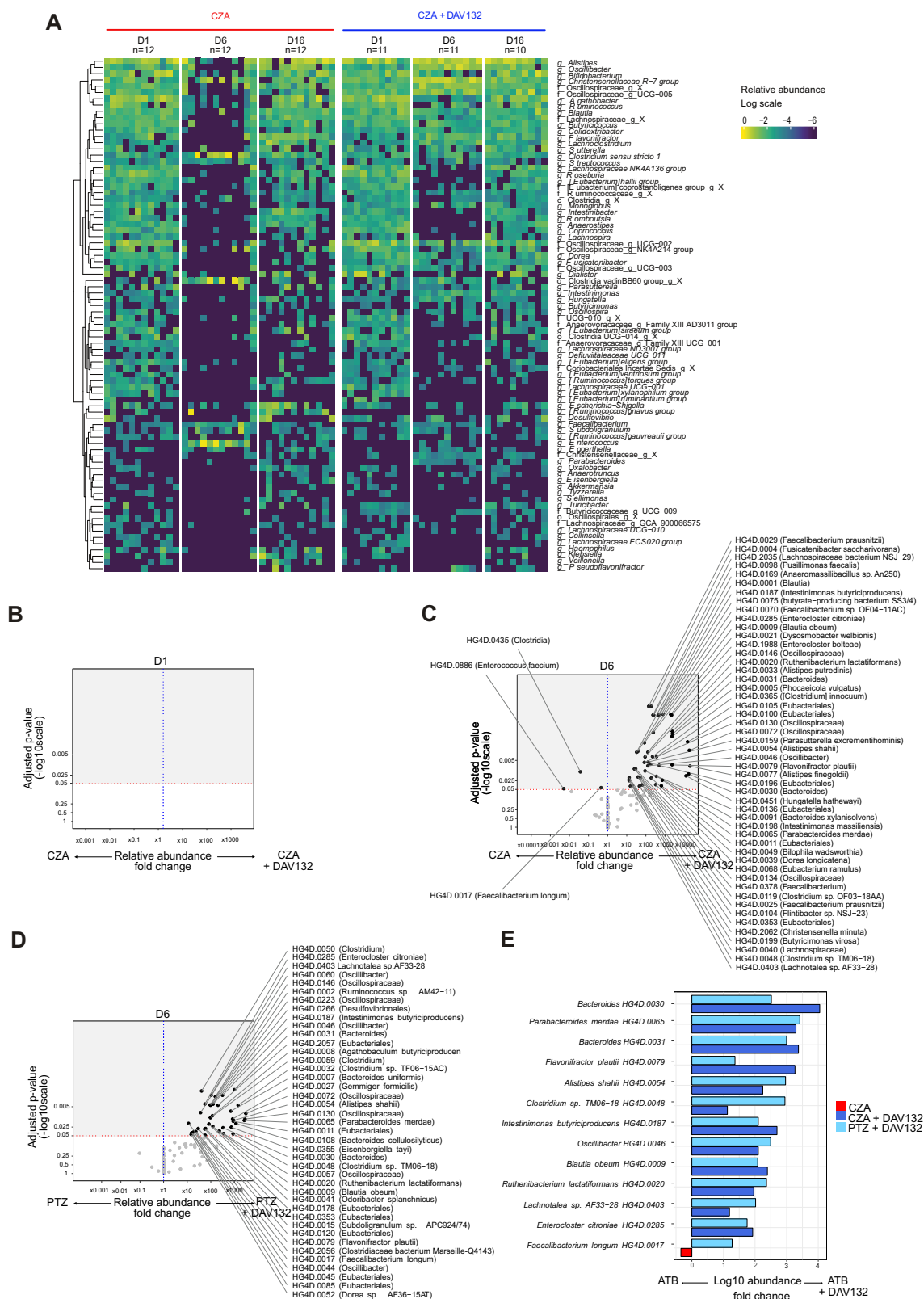
Fig. 3 | Impact of antibiotics alone or in combination with DAV132 12 g on microbiome composition in healthy volunteers (HV). A Heatmap comparing the global 16S rRNA intestinal microbiota of CZA vs. CZA + DAV132 over time from D1 to D16. Each column represents one HV included in the clinical trial. **B** Metagenomics microbiome profiling with volcano plot representation of the adjusted *p*-value versus the magnitude of change (fold change) of the Metagenomic Species relative abundance observed between CZA and CZA + DAV132 at D1, and at (**C**) D6 or (**D**) between PTZ and PTZ + DAV132 at D6. Dotted red line represents the significance threshold 0.05 used in the differential analysis. **E**. Common bacterial species found to be significantly different between CZA or PTZ and CZA or PTZ + DAV132. CZA ceftazidime-avibactam, D day, PTZ piperacillin-tazobactam, DAV132 DAV132 12 g po tid. Source data are provided as a Source Data file.
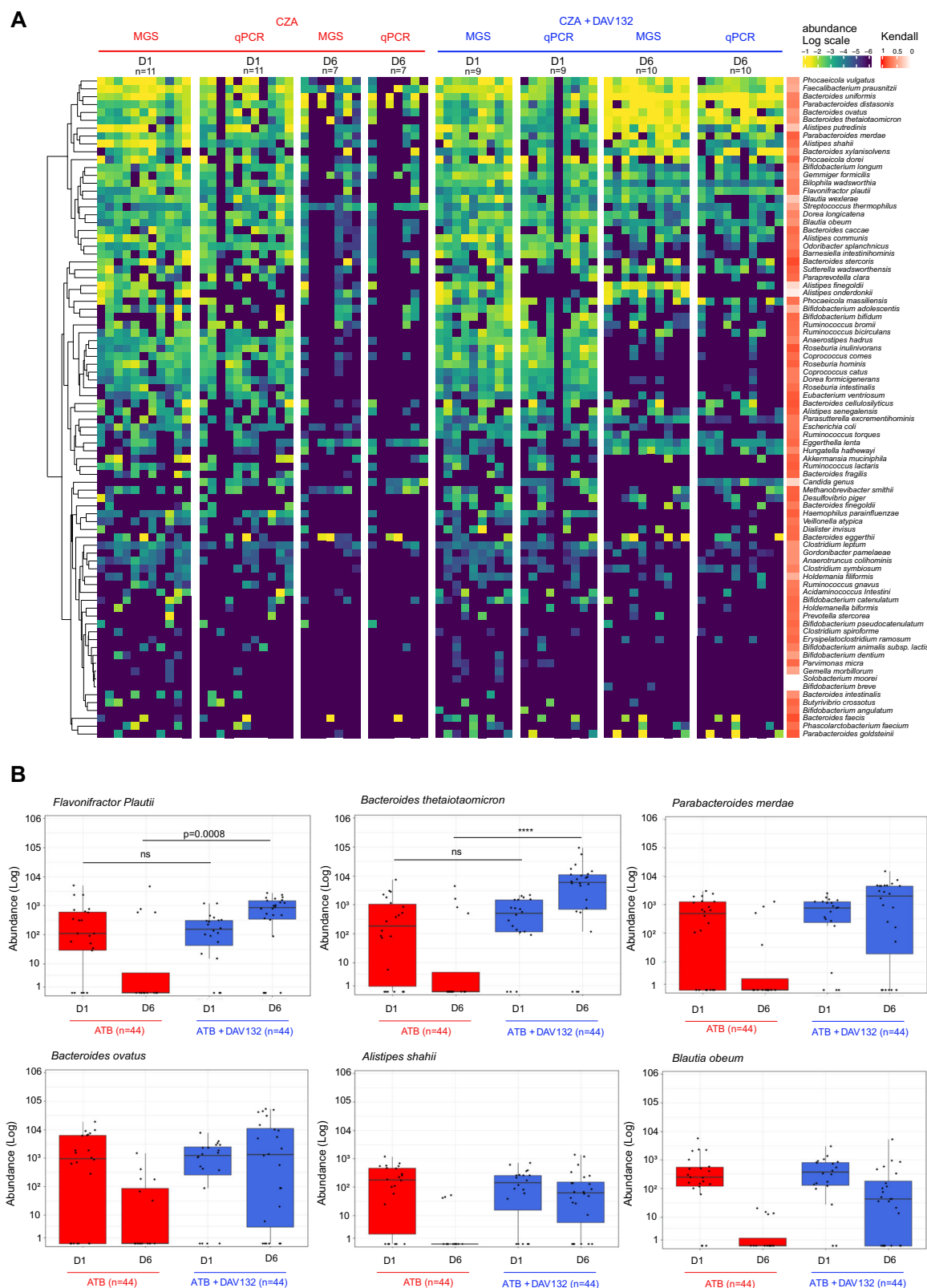
Fig. 4 | Correlation between qPCR panel and metagenomics on the microbiome evolution of healthy volunteers (HV) on the trial. A Heatmap aligning matching metagenomics and qPCR bacteria n = 84 of CZA D1, D6 and CZA + DAV132 D1 and D6. Kendal score represents the commonality between both sequencing strategies. Each column represents one HV. **B** qPCR normalized absolute representation of 6/ 12 common bacterial species found to be significantly different between CZA and PTZ vs CZA-DAV132 and PTZ + DAV132. Statistical test only performed between ATB vs ATB + DAV132 with a non-parametric Wilcoxon rank sum test. ATB antibiotic, CZA ceftazidime-avibactam, D day, DAV132 DAV132 12 g po tid. (ns non-significant, ****p < 0.0001). Source data are provided as a Source Data file.
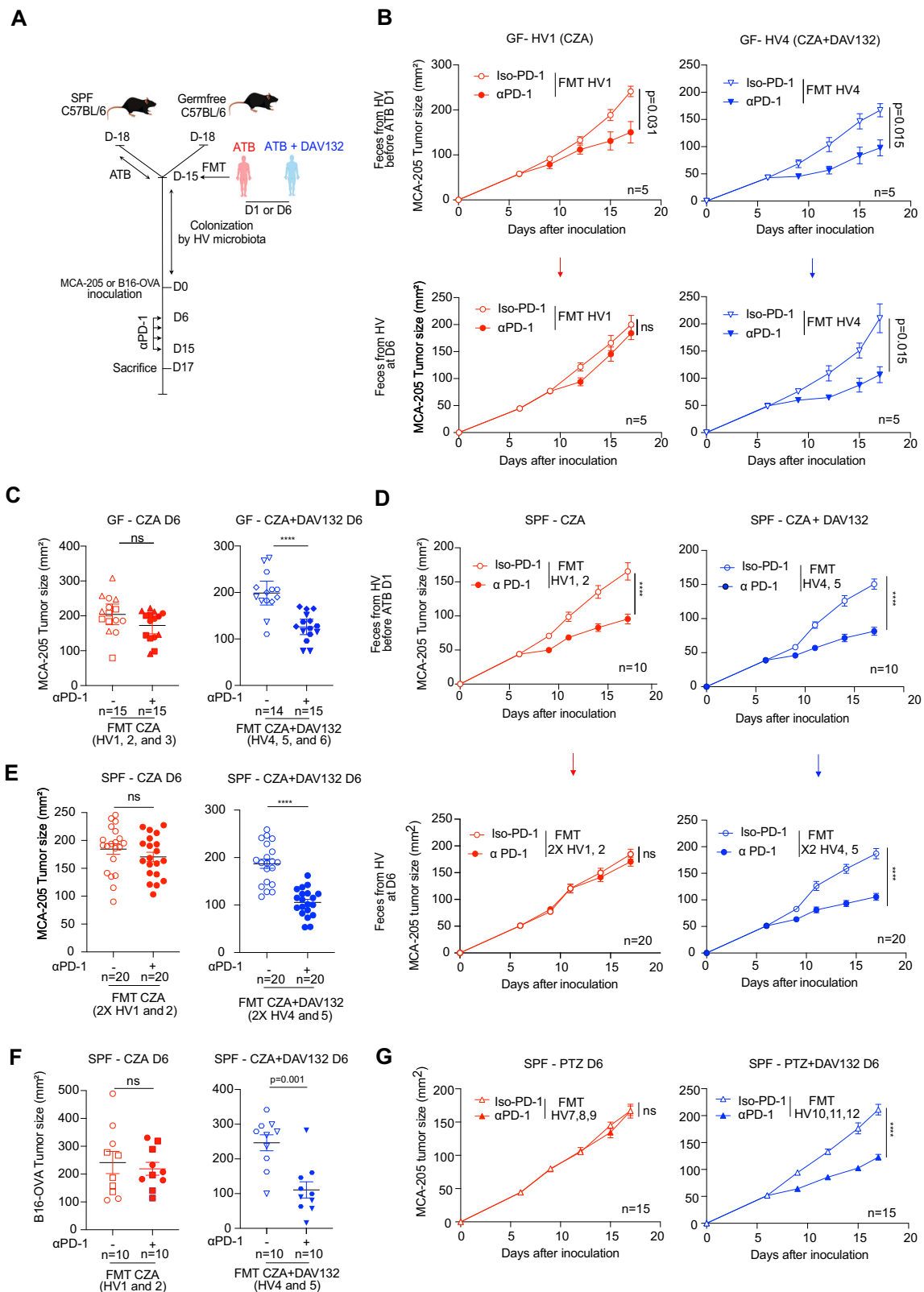
partially protected microbiome diversity and composition, and maintained several bacterial taxa associated with ICI response[24]. Using avatar murine tumor models, we were able to demonstrate that the protective effects of DAV132 against ATB-related dysbiosis are sufficient to maintain the anti-response to anti−PD-1. This anti-tumor activity was medicated by an upregulation of cytotoxic CD8^{+} T cells in the TILs. For CRO, due to the presence of β-lactamase, the concentration of fecal CRO were modest and did not lead to a significant ATB-related dysbiosis.

This finding extends prior results obtained from HV and hospitalized patients treated with fluoroquinolones who received DAV132 at a dose of 7.5 g po tid[33]. Extensive pharmacokinetic monitoring demonstrated no impact of co-administration of DAV132 on the plasma exposure of either CZA or PTZ (ATB and β-lactamase

Fig. 5 | Murine recolonization with feces from healthy volunteers (HV) on DAV132 protects αPD-1 response during CZA and PTZ treatment.
A Experimental design of avatar mice experiments. **B** Representative MCA-205 tumor growth curve in germ-free mice after FMT from HV, in the CZA group (HV1) at baseline D1 (upper panel) or D6 (lower panel), or from HV in the CZA + DAV132 group (HV4) at baseline D1 (upper panel) or D6 (lower panel), treated with Iso-PD-1 control or αPD-1 $n = 5$ mice/group. **C** Mean tumor size at sacrifice in MCA-205–inoculated germ-free mice at sacrifice following FMT from three HV on CZA (D6) and three HV on CZA + DAV132 (D6). **D** Pooled MCA-205 tumour growth curves in ATB-treated mice post-FMT samples obtained at D6 in 2 HV who received CZA ($n = 10$ mice/group) or CZA + DAV132 in duplicate HV treated with Iso-PD-1 control or αPD-1 ($n = 20$ mice/group). **E** Mean tumor size in MCA-205–inoculated in ATB-treated mice at sacrifice following FMT from duplicated two HV on CZA (D6)

and duplicated two HV on CZA + DAV132 (D6). **F** Mean tumor size in B16-OVA–inoculated in ATB-treated mice at sacrifice following FMT from two HV on CZA (D6) and two HV on CZA + DAV132 (D6). **G** Pooled MCA-205 tumour growth curves in ATB-treated mice post-FMT samples obtained at D6 in 3 HV who received PTZ or 3 HV PTZ + DAV132 treated with Iso-PD-1 control or αPD-1 $n = 15$ mice/group. (Data are presented as mean ± SEM, the Mann–Whitney U test was used to determine significant differences among the different groups at the time of sacrifice. For **C–F**, **G**, each dot represents one mouse and each shape represents one HV. (ns non-significant; ****$p < 0.0001$). ATB antibiotic, CZA ceftazidime-avibactam, D day, FMT fecal microbiota transplantation, HV healthy volunteer, ns not significant, PTZ piperacillin-tazobactam, DAV132 DAV132 12 g po tid. Source data are provided as a Source Data file.

inhibitors) at a higher dose of 12 g tid. Conversely, DAV132 reduced the concentration of ceftazidime and piperacillin to almost undetectable levels in fecal samples obtained from HV. The combination of 16S rRNA gene and shotgun metagenomic sequencing revealed that ATB elimination in the colon by DAV132 was associated with a significantly higher bacterial diversity, particularly at D6, and a more rapid return toward baseline diversity. In contrast, HV on ATB alone exhibited a profound decrease in diversity that had not fully recovered one month after ATB cessation. At the taxa level, DAV132 prevented the loss of more than 40 and 50 bacteria in the feces of PTZ-treated and CZA-treated HV, respectively. Post-ATB, DAV132 was able to preserve known immunogenic bacteria loss, such as *Ruminococcus*, *Eubacterium*, *Alistipes* and *Faecalibacterium prausnitzii* known to be repeatedly over-represented in patients who responded to αPD-1 therapy[3,8]. Despite not perfectly protecting the entire microbiota composition compared to control, we used two avatar murine tumor models to demonstrate that the microbiota composition of HV in the ATB + DAV132 groups had the necessary bacterial clusters to sustain αPD-1 activity.

Several research groups have attempted to use various strategies to overcome increased rapid recovery of gut microbiome composition post-ATB including consortium of bacteria. Suez et al. reported in HV receiving oral ciprofloxacin and metronidazole that daily oral supplementation with an 11-strain probiotic induced a markedly delayed and persistently incomplete microbiota restoration compared to HV who were allowed to spontaneously recover their microbiota[25]. In addition, HV who received autologous FMT from a sample collected pre-ATB had a faster and near-complete recovery. In the same vein, Spencer et al. revealed that advanced melanoma patients amenable to ICI who used over-the-counter probiotics had a shorter progression-free survival[11].

Prior studies have shown that when co-administered with fluoroquinolone, DAV132 exerts a significant protective effect on intestinal microbiota diversity and composition, regardless of whether it is administered orally or intravenously[27,33]. Importantly, ATB-related dysbiosis is also known to lead to *C. difficile* and one of the objectives of the trial was to test DAV132 in HV treated with CRO because it is known to increase the change of developing *C. difficile*[36]. Beyond its potential in ICI, studies using a hamster model of lethal *C. difficile*-induced colitis[37] have shown that DAV132 preserves the intestinal microbiota and dose-dependently protects from death[28–30]. Furthermore, we showed using an ex vivo validated assay[38] that, whereas the feces of healthy subjects cannot be colonized by *C. difficile*, fluoroquinolone ATB treatments enable such colonization, and resistance to colonization is preserved in the feces of HV and those who receive DAV132 together with ATB[33].

Our present study has limitations. Firstly, we assessed the role of DAV132 in HV, while recent studies suggest that the development of cancer is associated with a deviated microbiota repertoire, also referred as cancer-dysbiosis, that correlates with an ileopathy[39]. Hence, further studies are needed to determine whether the beneficial effects of DAV132 are replicated in patients with cancer. Secondly, DAV132

treatment was initiated on the same day as the ATB, to have an immediate effect on ATB scavenging, and this may represent a challenge in routine oncology practice. Thirdly, we tested three broad-spectrum ATB. CRO hydrolysis by resident β-lactamase was able to prevent ATB-related dysbiosis therefore in this context DAV132 is not recommended. Fourthly, we did not characterize the origin of the upregulation of CD8+ cytotoxic T cells in TILs. Indeed, Fidelle et al. unraveled that in ATB-treated mice, recolonization of *Enterocloster genus* post-ATB exposure downregulated Mucosal vascular addressing cell adhesion molecule 1 (MAdCAM-1) the ligand of gut T cell homing receptor integrin α4β7. This downregulation led to an exodus of T regulatory cells (Tr17cell) in the tumor microenvironment and inhibition of ICI[40]. Lastly, our study evaluated DAV132 in HV treated with ATB, and our preclinical work focused on cancer models, we did not yet study DAV132 in cancer patients, limiting the generalization of this approach to patients with cancer. Nevertheless, our study highlights that a similar technology should be studied in patients with cancer. Therefore, further studies are needed to determine whether the beneficial effects of DAV132 are replicated in cancer patients. To note, Davolterra interrupted its operations due to a bankruptcy that was not due to limitations in DAV132 activity, or any unexpected adverse events related to DAV132. The interruption in operations at Davolterra was due to suboptimal clinical trial design in the *Clostridium difficile* space outlined in Vehreschild et al.[41]. In summary, this study provides a strong rationale for investigating the use of activated charcoal to prevent ATB-related dysbiosis in patients with cancer amenable to ICI.

Methods
Clinical trial
Trial design, treatment, and HV selection. CL-006 a randomized, open-label, parallel groups, controlled study assessing the effect of DAV132 capsule filed as medical device and not as a drug to the EUDAMED with the objective to determine the plasma concentration of three ATB (CZA, PTZ and CRO) alone or in combination with DAV132 at 2 different doses (7.5 g pot id or 12 g pot id x 7 days). Primary and secondary objective of HV on CRO are presented even if they are evaluated independently for another project related to *Clostridium difficile* infection[42]. The study has been conducted and completed from May 2019 to December 2019. The study protocol is available in the Supplementary Information file. The study was conducted in a phase 1 centre in France according to Medical Device regulation, approved by the board of le comité de protection des personnes (C.P.P.) Sud-Ouest et Outre-Mer I, and registered by Competent Authority l'Agence nationale de sécurité du médicament et des produits de santé (ANSM) under number: 2019-A00240-57. All investigations were conducted by investigators after HV had provided informed consent and all activities were performed according to Good Clinical Practice (GCP).

148 HV were randomized in a factorial plan assessing the concomitant use of DAV132 or not (CTRL) at 2 doses and ATB (CZA, PTZ, CRO or not (CTRL)). After randomization, HV were treated with (CZA, PTZ, CRO or not (CTRL)) over 5 days alone or in combination with DAV132 over
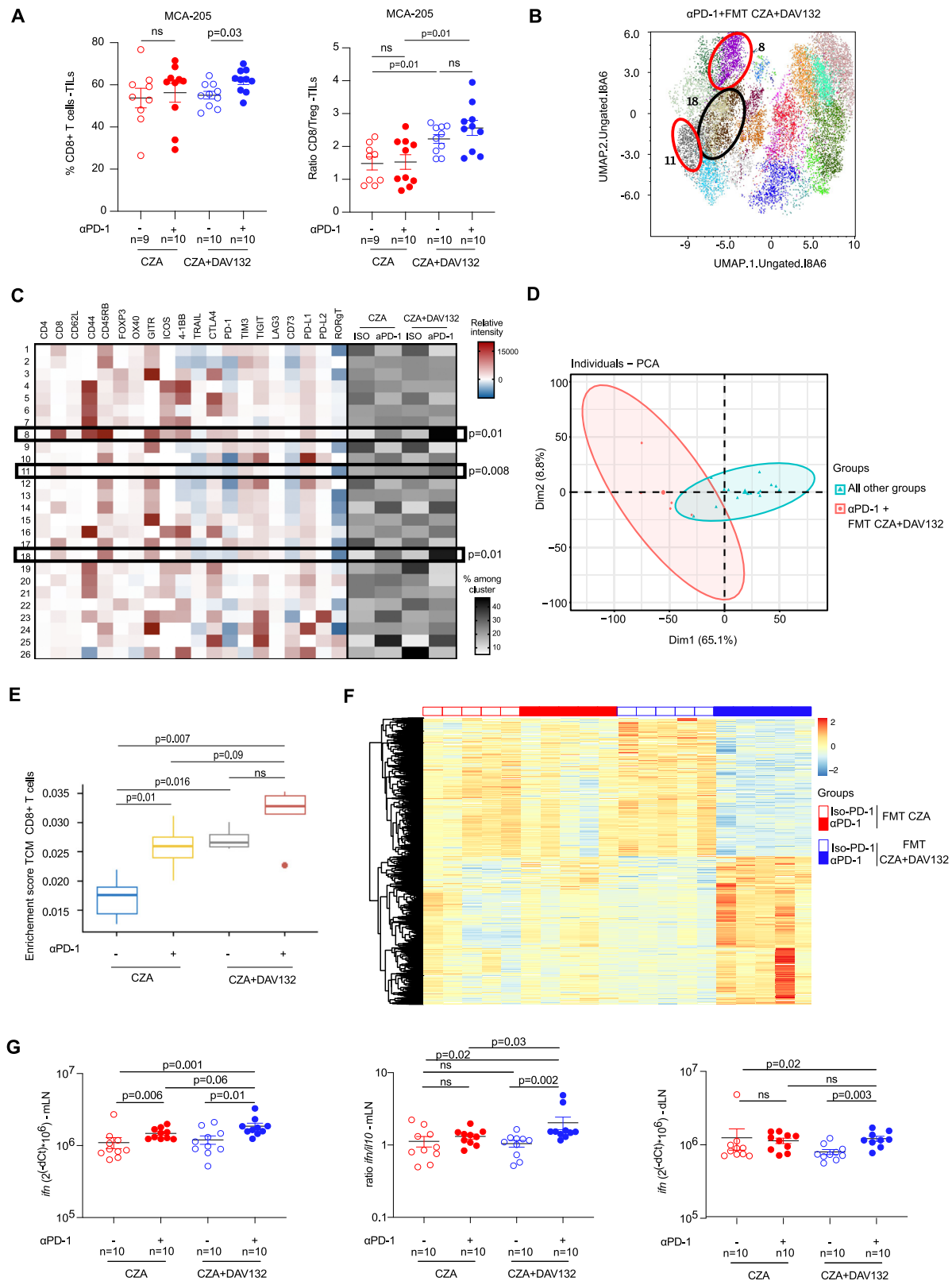
7 days. PTZ was administered at dose of 4 g/0.5 g every 8 h (q8h), ceftazidime/avibactam (CZA) at dose of 2 g/0.5 g every 8 h (q8h), and CRO was administered 1 g q 24. DAV132 was administered at a dose of 7.5 g or 12 g taken orally 3 times per day for a total duration of 7 days (Fig. 1A). Compliance was very good, only two HV did not reach 95% compliance and were therefore excluded from the analysis. HV were thereafter followed for one month for safety purpose.

To be eligible in the study, HV had to be aged 18-60 years old, body mass index (BMI) between 18.5 and 30 kg/m², normal physical examination with normal vital signs and a normal digestive transit, with usually at least one daily stool and have signed informed consent before any investigations. Exclusion criteria were mainly absence of significant medical history (Supplementary Table 3).

Fig. 6 | DAV132 maintains an effective immune response during ATB treatment in mice. A Flow cytometry analysis of the total CD8⁺Tcells and the ratio of CD8⁺ T cells/Treg population in MCA-205 tumor infiltrating lymphocytes (TILs) from ATB-treated mice recolonized with FMT from D6 samples in four HV (1, 2, 4, and 5) who received CZA alone or CZA + DAV132 at D6 (Fig. 5D, E). Data are presented as mean ± SEM, the Mann–Whitney *U* test was used to determine significant differences among the different groups. Each dot represents one mouse. **B** From experiment presented in Fig. 5D, E, UMAP visualization of tumor-infiltrating T cells in the group FMT CZA + DAV132 (Iso-PD-1 or αPD-1) **C** Heatmap representation of the 26 populations visualized in the UMAP with their respective normalized mean fluorescence intensity of the depicted markers. In grey, the frequency of pooled population for each group and the statistical analysis were done based on the percentage per mouse. **D** RNAseq of the bulk tumor representing the FMT from CZA-DAV132 + αPD-1 compared to the 3 other groups. *n* = 5mice/group, samples depicted in first two principal components space. For each of the 2 axes, values

within parentheses correspond to explained variance. Ninety-five percent confidence ellipses were added. **E** ImmuCellAI-mouse extrapolation of central memory CD8⁺ T cells. The center line indicates the median value, lower and upper hinges represent the 25th and 75th percentiles, respectively, and whiskers denote minimum and maximum. **F** RNAseq heatmap representing expression of genes differentially expressed on MCA-205 CD8⁺ T cells sorted *n* = 5mice/group between CZA-DAV132 + Iso-PD-1 and CZA-DAV132 + αPD-1 and other groups (FDR adjusted *p* < 0.01). Rows: genes were clustered based on Euclidean distance and « complete » method. Columns: samples were ordered given group membership. **G** qPCR of *ifng* gene and *the ifng/il-10* ratio in the mesenteric lymph nodes and draining lymph node from the 4 experimental groups, Data are presented as mean ± SEM, the Mann–Whitney *U* test was used to determine significant differences among the different groups. CZA ceftazidime-avibactam, FMT fecal microbiota transplantation, *infg interferon gamma*, il10 *interleukine-10*, PD-1 programmed cell death protein 1, PTZ piperacillin-tazobactam, DAV132 DAV132 12 g po tid. (ns non-significant).

Objectives and endpoints. The primary objective was to assess the effect of DAV132 either at 7.5 g or 12 g pot id on the plasma concentration of β-lactams at steady-state (AUC0-τ) and compared it to HV treated with the same ATB and not receiving DAV132.

Secondary objectives were assessment of safety (proportion of HV having at least one AE), assessment of potential interaction of DAV132 on the fecal excretion of β-lactam. Exploratory objectives included the protective effect of DAV132 on the intestinal microbiome diversity using 16S rRNA and metagenomics for the timepoints represented in Fig. 1A.

Plasma samples were collected on D1 and D5 prior to ATB infusion and at predefined timepoints thereafter until 8 h after infusion to measure pharmacokinetic parameters. Fecal samples were prospectively collected at baseline, daily from D2 to D9, and at D9, D12, D16, D25 and D37.

Statistics. AUC0-τ of piperacillin, tazobactam, ceftazidime, avibactam and ceftriaxone plasma levels after the last dose at D5 of PTZ, or of CZA, or CRO were calculated for subjects receiving DAV132, at 7.5 g tid or 12 g tid with β-lactam, and for those receiving the same β-lactam regimen without DAV132. Within each β-lactam arm, and separately for each β-lactam, AUC0-τ of piperacillin, tazobactam, ceftazidime, avibactam, and ceftriaxone plasma levels after the last dose at D5 of PTZ, of CZA or CRO were calculated. τ was defined as the time interval between two administrations (8 h for PTZ and CZA, 24 h for CRO). For each β-lactam, the two groups (DAV132 12 g, and no DAV132) were compared using an analysis of variance (ANOVA) on log-transformed AUC0-τ. The darkening of stools due to DAV132 was analysed between the first intake of DAV132 and the darkening of the stools (T1) and between the last intake of DAV132 and the return to the usual colour of stools (T2). The duration of each time intervals (T1 and T2) was described in each group receiving DAV132 7.5 or 12 g tid. A two-factor ANOVA was performed over the 8 groups receiving DAV132 to analyse the effect of DAV132 7.5 g or 12 g, of the co-administration of β-lactams or no β-lactam, and of their interaction.

No formal statistical calculation of the number of subjects was performed. A sample size of 12 evaluable subjects per group was considered adequate for the analysis of the primary endpoint, according to the variability of each of the two β-lactams PK after repeated administration. HV were allocated to treatment groups in a 1:1 ratio from a computed randomization list generated by an independent statistician. Block size in randomization was of 12 subjects. No blind was implemented in the trial.

Statistical analyses (demographics, safety, efficacy/performance, and exploratory data) were performed using SAS® version 9.4 (SAS Institute Inc., Cary, NC, USA). The Chi-squared test was used to compare differences in toxicities. Antibiotic PK parameters were calculated using Phoenix® WinNonlin® version 8.1 (Certara USA, Inc., Princeton, NJ).

AUC_{D1-DI6} of the changes from baseline of the Shannon index were calculated for subjects receiving DAV132, at 7.5 g or 12 g tid with β-lactam, for those receiving the same β-lactam regimen without DAV132 and for those receiving no treatment. For each β-lactam, the three groups were compared using an analysis of variance (ANOVA) followed by pairwise comparisons.

Principal Coordinates Analysis (PCoA) was performed to assess β-diversity based on Bray–Curtis dissimilarity index between groups and permutational multivariant analysis of variance (PERMANOVA) was used to determine statistical differences between groups at each timepoint.

Bray–Curtis distances between subjects of the DAV132 group or no DAV132 group and subjects of the control groups were compared for each β-lactam at each timepoint with a linear mixed model where treatment group was the fixed effect.

Differences in the relative abundance of microbial community members were assessed for significance using non-parametric tests (Kruskal–Wallis or Wilcoxon rank sum test according to group comparisons) controlling for false-discovery rate (FDR) with Benjamini-Hochberg test. The rank-biserial correlation was applied to determine effect size with a 95% CI. Threshold of statistical significance was established at *p* = 0.05.

Plasma and fecal antibiotic and β-lactamase inhibitor concentration measurements

Determination of Ceftazidime (CZA), Avibactam (AVI) and simultaneous determination of Piperacillin (PIP) and Tazobactam (TAZ) or Ceftriaxone (CRO) in EDTA-plasma and in human feces were carried out LC-MS/MS assays, the conditions of which are detailed hereafter.

Sample preparation. The EDTA plasma samples were prepared by protein precipitation: For each analyte, an aliquot of EDTA plasma sample was spiked with Internal Standard (IS) working solution and extracted with 3 to 4 volumes of acetonitrile. After centrifugation, the supernatant fluid was evaporated until dry, and the residue reconstituted in solvent for LC-MS/MS analysis. The IS working solutions and reconstitution solvents are detailed in Supplementary Table 4. The preparation of fecal samples was done by extraction of a feces aliquot with three volumes of 50 mM sodium phosphate buffer pH 7.0 containing 80 mM NaCl, centrifugation and filtration through 0.45 μm Nanosep MF GHP centrifugal devices to afford a free fraction feces filtrate. The filtrate was then either diluted or spiked with IS solution, and subjected to liquid-liquid extraction, as described in Supplementary Table 4.

UHPLC conditions. Gradient UHPLC methods, the conditions of which are detailed in Supplementary Table 5, were used for the determination of CZA, AVI and PIP/TAZ in plasma and feces samples.
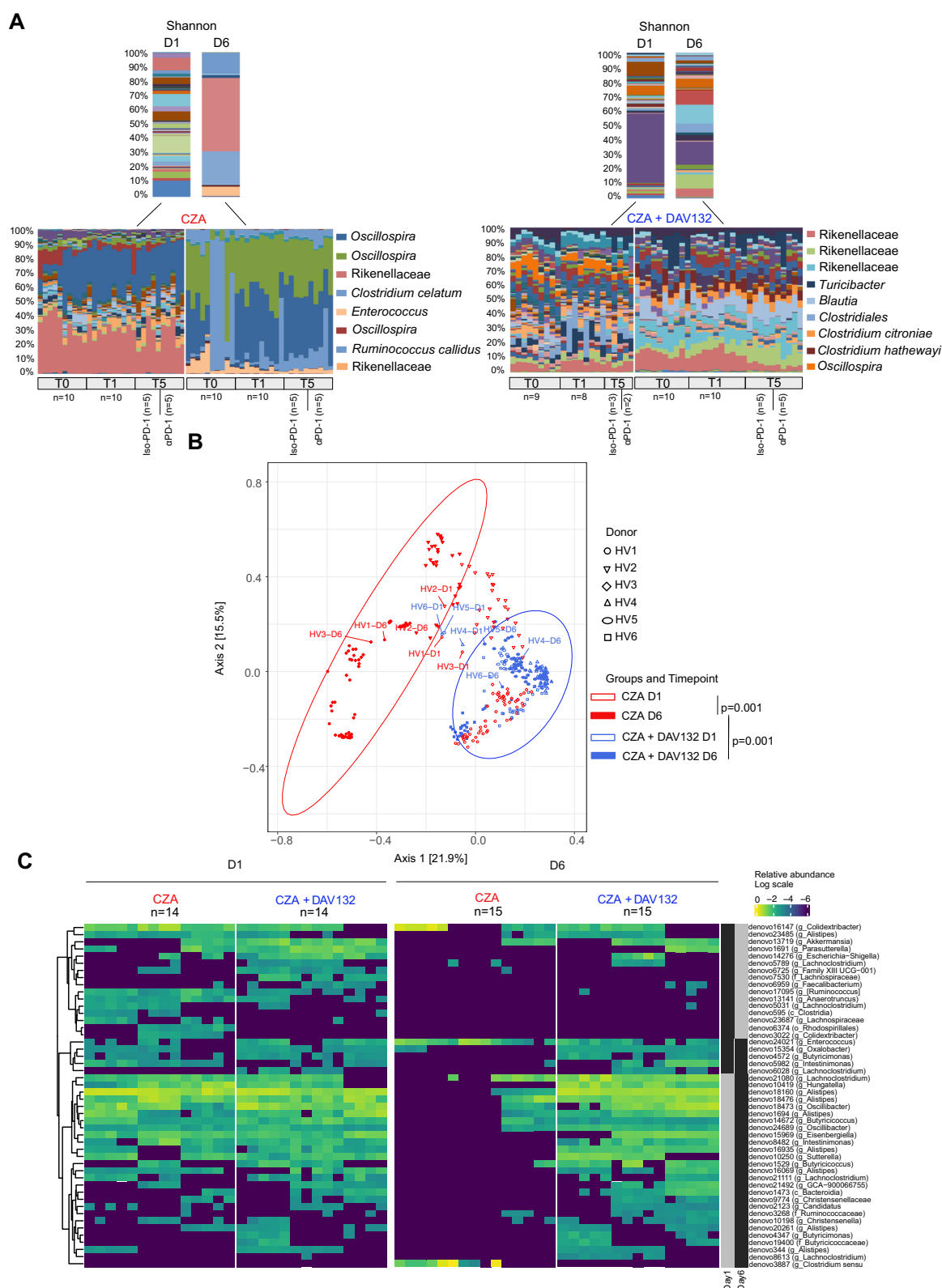
Mass spectrometric conditions. The mass spectrometer was an API 4000 (Applied Biosystems) and was operated with the conditions described in Supplementary Table 5.

DNA extraction from human or mice fecal samples
Microbial DNA was extracted from 100 mg of feces collected from either HV, or germ-free mice transplanted with stools from selected HV,

from the CL-1006 clinical trial using an optimized protocol partially based on commercially available extraction kits (QIAamp DNA stool Kit, Qiagen, Germany) with the addition of chemical and mechanical lysis steps (GenoScreen, Lille, France). Negative controls (Extraction protocol applied on sterile water) were regularly introduced. Extracted DNA was quantified using an in-house methodology based on the use of DNA fluorometric intercalant (SYBR® Green I, Sigma-Aldrich).

Fig. 7 | Correlation of the murine microbiota post-FMT. A Compositional histograms of two representative examples of the gut microbiota composition determined with 16S rRNA sequencing for the HV donor collected at D1 or D6 of CZA vs CZA + DVA132 compared to the gut microbiota mice post-FMT with these feces samples at different timepoints; T0 (tumour inoculation), T1 (before start of the treatment) T5 (after four αPD-1 or isotype control cycles). Left panel represents on top the HV1 microbiota composition before (D1) and after (D6) CZA treatment and below, recolonized murine fecal samples collected during experiment. Right panel represents HV5 before (D1) and after (D6) CZA + DAV132 treatment. In the lower panels, each column represents one fecal sample. **B** Principal coordinates

analysis (PCoA) analysis based on Bray–Curtis distances of HV donor and matching murine fecal samples collected after four cycles of αPD-1 or isotype control (D17 on the Fig. 5A). Each color corresponds to one treatment at one timepoint and each shape to one HV donor. A PERMANOVA test was applied to test statistical differences between groups. **C** Heatmap comparing fecal samples from germ-free mice after two αPD-1 administrations (D12) following FMT from HV donors who were on CZA alone or CZA + DAV132 obtained at D1 or D6. Each column represents one mouse. CZA ceftazidime-avibactam, D day, FMT fecal microbiota transplantation, HV healthy volunteer, PD-1 programmed cell death protein 1, DAV132 DAV132 12 g po tid. Source data are provided as a Source Data file.

16S rRNA gene pyrosequencing and data pre-processing

The hypervariable V3-V4 region of the 16S rRNA gene (16S; 5′-TACG-GRAGGCAGCAG-3′ and 5′-CTACCNGGGTATCTAAT-3′) was amplified using an optimized and standardized amplicon-library preparation protocol (Metabiote®, GenoScreen, Lille, France). Positive (Artificial Bacteria Community comprising 17 different bacteria (ABCv2)) and negative (sterile water) controls were also included. Briefly, PCR reactions were performed using 5 ng of genomic DNA and in-house fusion barcoded primers (at 0.2 μM final concentrations), with an annealing temperature of 50 °C for thirty cycles. PCR products were purified using Agencourt AMPure XP magnetic beads (Beckman Coulter, Brea, CA, USA), quantified according to GenoScreen's protocol, and mixed in an equimolar amount. Sequencing was performed using 250-bp paired-end sequencing chemistry on the Illumina MiSeq platform (Illumina, San Diego, CA, USA). Raw paired-end reads were then demultiplexed per sample and subjected to the following process: (1) search and removal of both forward and reverse primer using CutAdapt 2.0, with no mismatches allowed in the primer's sequences; (2) quality-filtering using the PRINSEQ-lite PERL script (v0.20.4), by truncating bases at the 3′ end with Phred quality score <30; (3) paired-end read assembly using FLASH, with a minimum overlap of 30 bases and > 97% overlap identity.

Taxonomic affiliation and diversity analyses from 16S rRNA gene data

Taxonomic and diversity analyses were performed with the Metabiote Online v2.0 pipeline (GenoScreen, Lille, France) that is partially based on the software QIIME v1.9.1. Following the pre-processing, the full-length 16S rRNA sequences were analysed and chimeric sequences were removed from the dataset (in-house method based on the use of USEARCH v8.1 algorithm). Then, a clustering step was performed in order to group similar sequences with a nucleic identity defined threshold (97% identity for an affiliation at the genus level on the V3-V4 regions of the 16S rRNA gene) with Uclust v1.2.22q through an open-reference operational taxonomic unit (OTU) picking process and complete-linkage method, finally creating groups of sequences or OTUs. An OTU cleaning step based on the data obtained for the ABCv2 community was performed. The most abundant sequence of each OTU was considered as the reference sequence of its OTU and was then taxonomically compared to a reference database (SILVA, release 138.1[17];). Various diversity indices were computed using QIIME v1.9.1. α-diversity indices (within-sample) and β-diversity (between-sample) were used to examine changes in microbial community structure. Measurement of α-diversity was done with the Shannon diversity index and Bray–Curtis dissimilarity index was computed for β-diversity. The principal coordinates analysis (PCoA) method was used to visualize group overall microbial differences.

Shotgun metagenomic sequencing

The sequencing of metagenomes was performed starting with ~50 ng of microbial DNA previously extracted for 16S rRNA profiling. Briefly, the genomic DNA was randomly sheared into fragments of around

350 bp using ultrasonic interruption (Bioruptor Pico, Diagenode SA). Short and large DNA fragments were removed using magnetic bead size selection and final profile was verified by capillary gel electrophoresis. The fragmented DNA was then used for library construction using the library preparation reagent kit (New England Biolabs) according to the service provider's protocol (Novogene, UK). Dual indices and adapter sequences were added to each sample during library construction and the final fragment distribution was evaluated using the HT DNA NGS 3 K assay (Perkin-Elmer, Cat# CLS960013), quantified by real-time PCR before library pooling and sequenced using 2 × 150 bp paired-end sequencing on the Illumina Novaseq 6000 system (Illumina, USA)

Sequencing data processing

On average, 21.7 million read pairs (~ 3 Gb) were generated per sample. Raw FASTQ files were filtered to remove host contamination by discarding read pairs in which either read maps to the human reference genome GRCh38 with Bowtie2[43](v 2.4.2). Reads were then trimmed to remove adapters and bases with a Phred score below 20 using AdapterRemoval[44] (v 2.3.1). Read pairs in which both reads passed filtering with a length of at least 100 bp were retained (High-Quality microbiome reads).

As the bioinformatic pipeline, acme-map version 4.2.1 (released 17 January 2022) was used with the gene catalog Hg04 (released 18 February 2021), MGS definitions HG4.D (released 22 June 2021), and MGS taxonomic annotations HG4D.2.2 (released 3 February 2022). On average, 85.4% of the High-Quality microbiome reads were then mapped to the gene catalog Hg04 using BWA mem (v. 0.7.17)[45]. An individual read was considered mapped to a gene if the mapping quality (MAPQ) was ≥ 20 and the read aligned with ≥ 95 % identity over ≥ 100 bp. A gene count table was consequently created with the number of mapped read pairs for each gene. Metagenomic species (MGS) were then identified based on the co-abundance of genes across the samples, following the method defined of Nielsen and colleagues[46]. For each MGS, a signature gene set was defined as the 100 genes optimized for accurate abundance profiling of the MGS. An MGS count table was created by counting the number of reads uniquely mapped to the MGS signature genes per sample. An MGS was considered detected if reads from a sample uniquely mapped to at least three of its signature genes; measurements that did not satisfy this criterion were set to zero. The MGS count table was normalized according to effective gene length and then normalized sample-wise to sum to 100 %, resulting in relative abundance estimates for each MGS. Downsampled (rarefied) MGS abundance profiles were calculated by random sampling, without replacement, of a fixed number of signature gene counts per sample, and then following the procedure described above. In this study, 35,373 signatures gene counts were sampled (the lowest for any analytical sample, thus not excluding any samples).

Differential analyses were performed as follow: a non-parametric test was used as relative abundances data do not follow a normal distribution. As the set of data is important and will necessarily lead to an over-correction for multiple parallel testing, we applied a filter on

microbial features and only kept those presenting a 50% prevalence in at least one group at one timepoint. To compare the groups CZA and CZA + DAV132, we used a Wilcoxon sum-rank test with calculation of exact p-values using R coin package. Adjusting the alpha error rate for multiple tests were conducted (one test per taxa). Adjustment was done using the Benjamini-Hochberg method with a false discovery rate (FDR) set to 5%. Outputs were summarised with Volcano plots and heatmaps.

To generate global heatmaps, all selected samples and species were plotted on a heatmap with a colour scale representing the microbial features species relative abundance after log10 transformation. A dissimilarity matrix based on Euclidean distances is then generated and clustered using "ward D2" hierarchical clustering methods of base R package. Dendrograms generated by the algorithm were used to plot the heatmap. Same clustering was applied, when applicable, to order samples within a group/timepoint. The hierarchical clustering dendrogram was then cut at a certain level in order to create a predefined number of clusters.

Cell culture, reagents, and tumor cell lines for mouse experiments

MCA-205 fibrosarcoma cells and B16-OVA melanoma, class I MHC H-2b syngeneic cell lines for C57BL/6 mice were used for this study. MCA-205 and B16-OVA cells were cultured as previously described[15]. All cultures were checked for Mycoplasma using PlasmoTest Mycoplasma Detection Kit (InvivoGen).

Murine experiments

All animal studies were approved by the Institutional Animal Care Committee (CIPA) and carried out in compliance with the Canadian Council on Animal Care guidelines. Murine experiments were conducted using seven-week-old female wild type C57BL/6 mice, obtained from Charles River. Germ-free female C57BL/6 mice were purchased from the International Microbiome Centre Germ-Free Facility (University of Calgary, Canada) and maintained at the Centre de recherche du Centre hospitalier de l'Université de Montréal (CRCHUM) germ-free facility.

Wild-type C57BL/6 mice were housed in sterile IVC at 21–23 °C, 40%-60% humidity, and on a 12 h light/dark cycle. Mice had free access to water and feed (Teklad global2918, Envigo Indianapolis, IN, USA). C57BL/6 germfree mice were housed in Sealed Positive Pressure IVC (Sentry SPP, Allentown, NJ, USA) in an exclusive holding room with the same environmental parameters as described above. Mice had free access to sterile water and 40 kGy irradiated feed (SAFE R03-40, Augy, France).

As previously published[15], after one week of acclimation at the CRCHUM animal facility, mice received an FMT performed by thawing fecal material at baseline (D1) or D6 of treatment from six different HV enrolled in the clinical trial DAV132-CL-1006. For the FMT experiments in SPF-reared mice, mice received three days of ATB solution containing ampicillin (1 mg/mL), streptomycin (5 mg/mL), and colistin (1 mg/mL; Sigma-Aldrich), which was added to the sterile drinking water of mice prior to FMT. Two weeks after FMT, mice were implanted subcutaneously with 0.8×10^6 MCA-205 cells or 0.5×10^6 B16-OVA cells, kindly provided by Dr. John Stagg (CRCHUM). When tumors reached 25 to 35 mm² in size, mice were treated four times intraperitoneally every three days with αPD-1 mAb (250 µg/mouse; clone RMP1-14, Bio X Cell) or isotype control (clone 2A3, Bio X Cell). The maximum size permitted by the ethics committee is 300 mm². Some of the tumours exceeded this size. Following clinical monitoring of these mice, and in the absence of animal suffering and any signs of deteriorating health, authorization was granted by the animal facility staff, veterinarians, and approval from the ethics committee to keep the mice. We were able to maintain them for a few additional days until the scheduled sacrifice date.

Flow cytometry analysis of immune cells

Tumors were harvested 11 days after the first injection of anti-PD-1 (αPD-1) in mice bearing MCA205 or B16-OVA tumors. TILs suspensions were prepared as previously published[15]. Two million tumor cells were preincubated with purified anti-mouse CD16/CD32 (clone 93; eBioscience, dilution 1:250) for 30 min at 4 °C before membrane staining with anti-mouse antibodies (Biologend) used for the panel anti-CD3 (clone 145-2C11, dilution 1:100), anti-CD45 (clone 30-F11, dilution 1:100), anti-CD8 (clone 53-6,7, dilution 1:200), anti-CD4 (Clone GK1.5, dilution 1:100). For intracellular staining, the FOXP3 staining kit (eBioscience) and anti-mouse anti-Foxp3 (Clone FJK-16s, eBioscience, dilution 1:150) was used. Dead cells were excluded using the Live/Dead Fixable Aqua Dead Cell Stain Kit (Life Technologies). The gating strategy is detailed in Supplementary Fig. 4C. Samples were acquired on a BD Fortessa 16-color cytometer (BD), and analyses were performed with FlowJo software (BD). For the panel 2, the following anti-mouse antibodies were used, anti-CD3 (Clone 145-2C11, Biolegend, dilution 1:100), anti-CD45 (clone 30-F11, Biolegend, dilution 1:100), anti-CD8 (clone 53-6,7, Biolegend, dilution 1:200), anti-CD4 (Clone GK1.5, Biolegend, dilution 1:100), anti-CD44 (Clone IM7, BD Biosciences, dilution 1:200), anti-TIGIT (Clone 1G9, BD Biosciences, dilution 1:100), anti-OX40 (Clone OX-86, BD Biosciences, dilution 1:100), anti-ICOS (Clone 7E.17G9, BD Biosciences, dilution 1:100), anti-CD73 (Clone TY/11.8, BD Biosciences, dilution 1:200), anti-PD-L1 (Clone MIH5, BD Biosciences, dilution 1:100), anti-TIM3 (Clone B8.2C12, BD Biosciences, dilution 50), anti-GITR (Clone YGITR 765, BD Biosciences, dilution 1:100), anti-4-1BB (Clone I17B5, BD Biosciences, dilution 1:100), anti-TRAIL (Clone N2B2, Biolegend, dilution 1:100), anti-CD45RB (Clone C363-16A, BD Biolegend, dilution 1:100), anti-PD-1 (Clone 29 F.1A12, BD Biosciences, dilution 1:150), anti-LAG3 (Clone C9B7W, BD Biosciences, dilution 1:100), anti-PD-L2 (Clone TY25, BD Biosciences, dilution 1:100), anti-CD62L (Clone MEL-14, BD Biosciences, dilution 1:100), anti-CTLA-4 (Clone UC10-4F10-11, BD Biosciences, dilution 1:150) and anti-mouse anti-FOXP3 (Clone FJK-16s, Thermofisher, dilution 1:150) ans RORgt (Clone B2D, Thermofisher, dilution 1:100) were used. Dead cells were excluded using the Live/Dead BD Horizon™ Fixable Viability Stain 575 V (BD Biosciences). Samples were acquired on a BD Symphony A5 29-color cytometer (BD), and analyses were performed with FlowJo software (BD). Gated total T cells (see gating strategy in Supplementary Fig. 4C) were down sampled and concatenated to export an equal number of normally distributed T cells from each sample for subsequent processing. Clustering was then performed using Phenograph (v2.5.0) 43 using default parameters (exclusive of the live/dead dye, CD3, CD45 markers), and Uniform Manifold Approximation and Projection (UMAP v4.0.4)44 was used for dimensionality reduction of the 26 identified clusters. Subsequently, ClusterExplorer v1.7.6 was used to integrate clustering strategies with all the markers with the exception of the live/dead dye, CD3, CD45 markers. Frequency of each subcluster was extracted for each individual mouse and GraphPad Prism was used for statistical analysis.

Specific bacteria probes for qPCR

Bio-Me's Precision Microbiome Profiling (PMP™) is a validated quantitative PCR method for analyzing the gut microbiota composition, based on TaqMan™ technology on OpenArray® format (Thermo Fisher Scientific). It targets 107 bacterial and archaeal species/subspecies and one fungal genus (Candida).

Standard curves for the assays were created using reference materials quantified by fluorescence (Quant-iT™ PicoGreen™ dsDNA Reagent, Thermo Fisher Scientific). The reference materials were acquired from DSMZ (Leibniz Institute, Braunschweig, Germany) or ATCC (American Type Culture Collection, Manassas, US). Standard curves for each qPCR assay were used to convert the quantification cycle (Cq) value into number of genomic copies per µL of sample; this number was transformed into normalized absolute quantification

(number of genomic copies per ng) by dividing it by the DNA concentration in each sample.

Among 88 samples, six had no measurable DNA and had to be excluded from the qPCR analysis, although it is important to note that these results were consistent with what was first obtained when performing 16S rRNA and metagenomic profiling. Five samples gave absolutely no PCR amplification among which 3 were also excluded from our dataset because their negative results were due to PCR inhibitors presence. These 5 specific samples were rerun to confirm results and, after these multiple quality controls, 79 samples were finally exploitable for this study.

All assays were validated in silico and in vitro for specificity and sensitivity, and in vitro for standard curve accuracy.

RNA extraction and RT-qPCR
mLN and dLN samples were snap frozen in liquid nitrogen in RLT Plus buffer containing 0.1% β-mercaptoethanol. On the day of extraction, samples were thawed at 4 °C and homogenized in a microtube homogenizer in RNA-free glass bead tubes. Total RNA extraction and genomic DNA removal were performed with the RNeasy Mini kit (Qiagen), following the manufacturer's recommendations. A maximum of 1 µg of RNA, measured using a Nano-DropTM Spectrophotometer (Thermo Fischer Scientific), was reverse transcribed into cDNA, using Maxima™ H Minus cDNA Synthesis Master Mix (ThermoFisher) following the manufacturer's recommendations.

Quantitative gene expression assay
The expression of mouse and human β2 microglobulin, *ifng, il10* (all from Life Technologies, with the references Mm00437762_m1, Mm01168134_m1, Mm01288386_m1, respectively) was analyzed with the TaqMan® Gene Expression Assay using the Universal Master Mix II on a StepOnePlus™ Real-Time PCR System (Life Technologies). Amplifications were carried out using the following ramping profile: 1 cycle at 95 °C for 10 min, followed by 45 cycles of 95 °C for 30 s, 60 °C for 1 min. Quantitative RT-PCR data were normalized to the expression levels of the housekeeping gene β2M, as indicated in each figure, by means of the $2 - \Delta Ct$ method multiplied by 10^6.

RNAseq sequencing
By using the Monarch Total RNA Miniprep kit (New England Biolabs), fifty nanograms of total RNA were ribodepleted with the RiboCop rRNA Depletion kit (Lexogen) by following manufacturer's protocol. Next, libraries were prepared with the SMARTer Ultra Low Input RNA for Illumina Sequencing kit (Takara) by following manufacturer's instructions. Built libraries were paired end (2*100 bp) sequenced on NextSeq2000 sequencing device (Illumina) with a depth of 25 million reads.

RNAseq data analysis
Raw FASTQ data were pseudo-aligned, and gene counts were quantified using Kallisto software (Bray et al.). Kallisto transcript index used as reference was built from merged human cDNA and ncDNA files from the GRCh37 assembly Ensembl. Gene-level count and transcripts matrices were then created with the DESeq2 library[47]. Low-count genes were pre-filtered by removing genes with too few reads; genes where there are not at least one sample with normalized counts greater than or equal to 5 were filtered out. Variant stabilizing transformation (VST) was then performed on normalized reads.

Genes differentially expressed were selected using the DESeq2 R package.

Principal component analysis (PCA) was used to cluster samples with shared profiles. This multivariate analysis simplifies the complexity in high-dimensional data projecting them onto lower dimensions called principal components. PCA were performed using VST counts using FactoMineR R package[48]. Only first 2 principal components were considered for representation.

Heatmap was performed using VST counts using pheatmap R package[49].

Tumor microenvironment (TME)-associated transcriptomic elements were quantified using ImmuCellAI-mouse tool[50], following corresponding guidelines. ImmuCellAI-mouse estimates the abundance of 36 immune cell types divided into three layers through a gene set signature-based method. Cells in layer 1 include three types of lymphoid lineage cells (B cell, NK cell and T cell) and four types of myeloid lineage cells (macrophage, DC, monocyte and granulocyte). Layer 2 is composed of subtypes of cells in layer 1, and cells in layer 3 are subtypes of CD4+ T and CD8+ T cells. Immune cell types differentially expressed between groups were selected with the Wilcoxon rank-sum test.

Statistical analysis for mouse experiments
SASv9.4 (SAS Institute, Cary, NC, USA) and PhoenixWinNonlin v8 (Certara, Radnor, PA, USA) were used for clinical data analyses. Post-hoc analyses (visualisation and statistics) were performed with R v4.2.1 (https://www.r-project.org/) and specific package of R program: Phyloseq v1.4 (https://joey711.github.io/phyloseq), Data.table v1.14.2 (https://CRAN.R-project.org/package=data.table), Dplyr v1.0.10 (https://CRAN.R-project.org/package=dplyr), Rstatix v0.7.0 (https://rpkgs.datanovia.com/rstatix/), ggplot2 v3.3.6 (https://ggplot2.tidyverse.org), lme4 v1.1-30 (https://github.com/lme4/lme4/), CompleHeatmap v2.12.1 (http://www.bioconductor.org/packages/devel/bioc/html/ComplexHeatmap.html), Coin v1.4-2 (http://coin.r-forge.r-project.org). Statistics are specified for each experiment.

For mouse experiments, data analyses were performed with GraphPad Prism 8 (GraphPad, San Diego, CA, USA). Tumor size differences and flow cytometry analysis parameters were calculated using non-parametric *t*-test. *P* values were two-sided with 95% confidence intervals: $*p < 0.05$; $**p < 0.01$; $***p < 0.001$. ns Non-significant.

Reporting summary
Further information on research design is available in the Nature Portfolio Reporting Summary linked to this article.

Data availability
The raw read data generated from the 16S rRNA sequencing from the fecal mouse samples in this study are available in the National Center Biotechnology Information Sequence Read Archive, under PRJNA897750 accession number. The raw read data generated from the 16S rRNA sequencing and metagenomic sequencing of the intestinal human microbiota in the clinical study are available in the National Center Biotechnology Information Sequence Read Archive, under accession number PRJNA922086. The raw read data generated from the RNAseq from tumor and CD8+ T cell sorted in this study were deposited in the NCBI Gene expression Omnibus and are available under GSE251922 accession number [https://www.ncbi.nlm.nih.gov/geo/query/acc.cgi?acc=GSE251922]. The study protocol is available in the Supplementary Information file. Additional individual deidentified participant data can be shared upon request to the corresponding author. All source data are provided with this paper with the exception of OTU and MGS tables that will be available from the authors upon reasonable request and with permission from the Bla-impact consortium. Contact details for access requests: bertrand.routy@umontreal.ca and meriem.messaoudene@umontreal.ca. The remaining data are available within the Article, Supplementary Information or Source Data file. Source data are provided with this paper.

References
1. Forde, P. M. et al. Neoadjuvant nivolumab plus chemotherapy in resectable lung cancer. *N. Engl. J. Med.* **386**, 1973–1985 (2022).

2. Haslam, A. & Prasad, V. Estimation of the percentage of US patients with cancer who are eligible for and respond to checkpoint inhibitor immunotherapy drugs. *JAMA Netw. Open* **2**, e192535 (2019).

3. Derosa, L. et al. Microbiota-centered interventions: the next breakthrough in immuno-oncology? *Cancer Discov.* **11**, 2396–2412 (2021).

4. Sepich-Poore, G. D. et al. The microbiome and human cancer. *Science* **371**, eabc4552 (2021).

5. Chen, D. S. & Mellman, I. Elements of cancer immunity and the cancer-immune set point. *Nature* **541**, 321–330 (2017).

6. Hanahan, D. Hallmarks of cancer: new dimensions. *Cancer Discov.* **12**, 31–46 (2022).

7. Routy, B. et al. Melanoma and microbiota: Current understanding and future directions. *Cancer Cell* S1535-6108(23)00431–2. https://doi.org/10.1016/j.ccell.2023.12.003 (2023).

8. Elkrief, A. et al. Antibiotics are associated with worse outcomes in lung cancer patients treated with chemotherapy and immunotherapy. *NPJ Precis. Oncol.* **8**, 143 (2024).

9. Routy, B. et al. Gut microbiome influences efficacy of PD-1-based immunotherapy against epithelial tumors. *Science* **359**, 91–97 (2018).

10. Derosa, L. et al. Intestinal Akkermansia muciniphila predicts clinical response to PD-1 blockade in patients with advanced non-small-cell lung cancer. *Nat. Med.* **28**, 315–324 (2022).

11. Spencer, C. N. et al. Dietary fiber and probiotics influence the gut microbiome and melanoma immunotherapy response. *Science* **374**, 1632–1640 (2021).

12. Lee, K. A. et al. Cross-cohort gut microbiome associations with immune checkpoint inhibitor response in advanced melanoma. *Nat. Med.* **28**, 535–544 (2022).

13. Derosa, L. et al. Gut bacteria composition drives primary resistance to cancer immunotherapy in renal cell carcinoma patients. *Eur. Urol.* **78**, 195–206 (2020).

14. Gopalakrishnan, V. et al. Gut microbiome modulates response to anti-PD-1 immunotherapy in melanoma patients. *Science* **359**, 97–103 (2018).

15. Messaoudene, M. et al. A natural polyphenol exerts antitumor activity and circumvents anti-PD-1 resistance through effects on the gut microbiota. *Cancer Discov.* candisc.0808.2021 https://doi.org/10.1158/2159-8290.CD-21-0808 (2022).

16. Baruch, E. N. et al. Fecal microbiota transplant promotes response in immunotherapy-refractory melanoma patients. *Science* **371**, 602–609 (2021).

17. Davar, D. et al. Fecal microbiota transplant overcomes resistance to anti–PD-1 therapy in melanoma patients. *Science* **371**, 595–602 (2021).

18. Routy, B. et al. Fecal microbiota transplantation plus anti-PD-1 immunotherapy in advanced melanoma: a phase I trial. *Nat. Med.* https://doi.org/10.1038/s41591-023-02453-x (2023).

19. Vétizou, M. et al. Anticancer immunotherapy by CTLA-4 blockade relies on the gut microbiota. *Science* **350**, 1079–1084 (2015).

20. Elkrief, A. et al. Antibiotics are associated with decreased progression-free survival of advanced melanoma patients treated with immune checkpoint inhibitors. *Oncoimmunology* **8**, e1568812 (2019).

21. Elkrief, A., Derosa, L., Kroemer, G., Zitvogel, L. & Routy, B. The negative impact of antibiotics on outcomes in cancer patients treated with immunotherapy: a new independent prognostic factor? *Ann. Oncol.* **30**, 1572–1579 (2019).

22. Pinato, D. J. et al. Association of prior antibiotic treatment with survival and response to immune checkpoint inhibitor therapy in patients with cancer. *JAMA Oncol.* https://doi.org/10.1001/jamaoncol.2019.2785 (2019).

23. Hakozaki, T. et al. The gut microbiome associates with immune checkpoint inhibition outcomes in patients with advanced non-small cell lung cancer. *Cancer Immunol. Res.* https://doi.org/10.1158/2326-6066.CIR-20-0196 (2020).

24. Thomas, A. M. et al. Gut OncoMicrobiome Signatures (GOMS) as next-generation biomarkers for cancer immunotherapy. *Nat. Rev. Clin. Oncol.* https://doi.org/10.1038/s41571-023-00785-8 (2023).

25. Suez, J. et al. Post-antibiotic gut mucosal microbiome reconstitution is impaired by probiotics and improved by autologous FMT. *Cell* **174**, 1406–1423.e16 (2018).

26. de Gunzburg, J. et al. Targeted adsorption of molecules in the colon with the novel adsorbent-based medicinal product, DAV132: a proof of concept study in healthy subjects. *J. Clin. Pharmacol.* **55**, 10–16 (2015).

27. de Gunzburg, J. et al. Protection of the human gut microbiome from antibiotics. *J. Infect. Dis.* **217**, 628–636 (2018).

28. Burdet, C. et al. Protection of hamsters from mortality by reducing fecal moxifloxacin concentration with DAV131A in a model of moxifloxacin-induced clostridium difficile colitis. *Antimicrob. Agents Chemother.* **61**, e00543–17 (2017).

29. Burdet, C. et al. Antibiotic-induced dysbiosis predicts mortality in an animal model of Clostridium difficile infection. *Antimicrob. Agents Chemother.* **62**, e00925–18 (2018).

30. Saint-Lu, N. et al. DAV131A protects hamsters from lethal Clostridioides difficile infection induced by fluoroquinolones. *Antimicrob. Agents Chemother.* **64**, e01196–19 (2019).

31. Shirley, M. Ceftazidime-avibactam: a review in the treatment of serious gram-negative bacterial infections. *Drugs* **78**, 675–692 (2018).

32. Perry, C. M. & Markham, A. Piperacillin/tazobactam: an updated review of its use in the treatment of bacterial infections. *Drugs* **57**, 805–843 (1999).

33. Vehreschild, M. J. G. T. et al. An open randomized multicentre Phase 2 trial to assess the safety of DAV132 and its efficacy to protect gut microbiota diversity in hospitalized patients treated with fluoroquinolones. *J. Antimicrob. Chemother.* **77**, 1155–1165 (2022).

34. Kaleko, M. et al. Development of SYN-004, an oral beta-lactamase treatment to protect the gut microbiome from antibiotic-mediated damage and prevent *Clostridium difficile* infection. *Anaerobe* **41**, 58–67 (2016).

35. Klastersky, J. et al. Management of febrile neutropaenia: ESMO Clinical Practice Guidelines. *Ann. Oncol. J. Eur. Soc. Med. Oncol.* **27**, v111–v118 (2016).

36. Wendt, S., Ranft, D., Rodloff, A. C., Lippmann, N. & Lübbert, C. Switching from ceftriaxone to cefotaxime significantly contributes to reducing the burden of Clostridioides difficile infections. *Open Forum Infect. Dis.* **7**, ofaa312 (2020).

37. Costello, S. P., Tucker, E. C., La Brooy, J., Schoeman, M. N. & Andrews, J. M. Establishing a fecal microbiota transplant service for the treatment of Clostridium difficile infection. *Clin. Infect. Dis. Publ. Infect. Dis. Soc. Am.* **62**, 908–914 (2016).

38. Harris, H. C. et al. Optimization of an assay to determine colonization resistance to Clostridioides difficile in fecal samples from healthy subjects and those treated with antibiotics. *Antimicrob. Agents Chemother.* **65**, e01401–20 (2020).

39. Yonekura, S. et al. Cancer induces a stress ileopathy depending on β-adrenergic receptors and promoting dysbiosis that contributes to carcinogenesis. *Cancer Discov.* **12**, 1128–1151 (2022).

40. Fidelle, M. et al. A microbiota-modulated checkpoint directs immunosuppressive intestinal T cells into cancers. *Science* **380**, eabo2296 (2023).

41. Vehreschild, M. J. G. T. et al. An obituary on DAV-132—authors' viewpoint on the current limits of pivotal trials in clinical microbiome research. *J. Antimicrob. Chemother.* **78**, 1551–1553 (2023).

42. Schulz, K. F., Altman, D. G., Moher, D. & CONSORT Group. CONSORT 2010 statement: updated guidelines for reporting

parallel group randomised trials. *J. Clin. Epidemiol.* **63**, 834–840 (2010).

43. Langmead, B. & Salzberg, S. L. Fast gapped-read alignment with Bowtie 2. *Nat. Methods* **9**, 357–359 (2012).

44. Schubert, M., Lindgreen, S. & Orlando, L. AdapterRemoval v2: rapid adapter trimming, identification, and read merging. *BMC Res. Notes* **9**, 88 (2016).

45. Li, H. & Durbin, R. Fast and accurate long-read alignment with Burrows-Wheeler transform. *Bioinforma. Oxf. Engl.* **26**, 589–595 (2010).

46. Nielsen, H. B. et al. Identification and assembly of genomes and genetic elements in complex metagenomic samples without using reference genomes. *Nat. Biotechnol.* **32**, 822–828 (2014).

47. Love, M. I., Huber, W. & Anders, S. Moderated estimation of fold change and dispersion for RNA-seq data with DESeq2. *Genome Biol.* **15**, 550 (2014).

48. Lê, S., Josse, J. & Husson, F. FactoMineR: an R package for multivariate analysis. *J. Stat. Softw.* **25**, 1–18 (2008).

49. Kolde, R. pheatmap: Pretty Heatmaps (2019).

50. Miao, Y.-R. et al. ImmuCellAI-mouse: a tool for comprehensive prediction of mouse immune cell abundance and immune microenvironment depiction. *Bioinforma. Oxf. Engl.* **38**, 785–791 (2022).

Acknowledgements

Author contributions

M.M.: conceptualization of murine experiments and murine analysis, data curation, formal analysis, microbiome analysis and interpretation, visualization, methodology, writing–original draft, project administration, writing–review and editing. S.F.: supervision of 16S and shotgun metagenomic experiments, data curation, formal analysis, visualization, methodology, writing–original draft, writing–review and editing. N.S.L.: conceptualization of murine experiments and murine analysis, methodology, formal analysis, writing-review and editing. M.P.: murine experiments. C.L.B.: data management, data curation, formal analysis, visualization, methodology, writing-review and editing. T.L.: microbiome data analysis and visualization. T.C.: operational management of 16S and shotgun metagenomic experiments, microbiome data analyses, writing–review and editing. C.F.: methodology and supervision of the clinical trial and pharmacokinetic measurements, data analysis, interpretation of the clinical results. K.B.: manufacture and quality control of DAV132, conception and supervision of analytical methods for pharmacokinetic analysis in blood and feces, data analysis. A.E.: writing-review and editing. M.I.: writing-review and editing. F.V.: conceptualization and supervision of the clinical trial and pharmacokinetic measurements, data analysis, interpretation of the clinical results, writing–review and editing. F.S.G.: conceptualization of murine and microbiome experiments, supervision, project administration, writing–original draft, writing–review and editing. L.B.: heled with flow cytometry analysis. A.A.: conceptualization of the clinical trial and microbiome analysis, editing. F.G., R.B., C.T.: performed RNAseq sequencing + analysis. J.G.: conceptualization of the clinical trial, supervision of the murine and microbiome experiments, writing-review and editing. B.R.: conceptualization, microbiome analysis and interpretation, formal analysis, supervision, writing–original draft, project administration, writing–review and editing.

Competing interests

B.R. and M.M. received research funding from Da Volterra to perform the experiments. B.R. receives grants from Kaleido, and Vedanta outside the submitted work, as well as consulting fees from BMS, AstraZeneca, Merck and Da Volterra. N.S.L., S.F., C.L.B., T.L., T.C., K.B., F.V., and F.S.G. are employees of Da Volterra. C.F., J.G. and A.A. are consultants for Da Volterra. All patents and patent applications resulting from PCT/EP2011/052682 and PCT/EP2019/071024 belong to Da Volterra. M.I. is an employee of Bio-Me. The remaining authors declare no competing interests.

Additional information

Supplementary information The online version contains supplementary material available at https://doi.org/10.1038/s41467-024-52373-8.

Correspondence and requests for materials should be addressed to Bertrand Routy.

Peer review information *Nature Communications* thanks Diwakar Davar and Xianghua Luo for their contribution to the peer review of this work. A peer review file is available.

Reprints and permissions information is available at http://www.nature.com/reprints

Publisher's note Springer Nature remains neutral with regard to jurisdictional claims in published maps and institutional affiliations.

Meriem Messaoudene[1], **Stéphanie Ferreira**[2], **Nathalie Saint-Lu**[2], **Mayra Ponce**[1], **Caroline Truntzer**[3,4], **Romain Boidot** ◉ [5], **Clément Le Bescop**[2], **Thomas Loppinet**[2], **Tanguy Corbel**[2], **Céline Féger** ◉ [2,6], **Karine Bertrand**[2], **Arielle Elkrief**[1,7],

Morten Isaksen [8], **Fabien Vitry**[2], **Frédérique Sablier-Gallis**[2], **Antoine Andremont**[2], **Lloyd Bod** [9], **François Ghiringhelli** [10], **Jean de Gunzburg** [2] & **Bertrand Routy** [1,7] ✉

[1]Axe Cancer, Centre de Recherche du Centre Hospitalier de l'Université de Montréal (CRCHUM), Montréal, QC, Canada. [2]Da Volterra, Paris, France. [3]Platform of Transfer in Biological Oncology, Georges François Leclerc Cancer Center-Unicancer, Dijon, France. [4]UMR INSERM 1231, Dijon, France. [5]Molecular Biology, Georges François Leclerc Cancer Center-Unicancer, Dijon, France. [6]Medical, EMI Biotech, Paris, France. [7]Hemato-Oncology Division, Centre Hospitalier de l'Université de Montréal (CHUM), Montréal, QC, Canada. [8]Bio-Me, Oslo, Norway. [9]Krantz Family Cancer Center, Center for Immunology and Inflammatory Diseases, Department of Medicine, Massachusetts General Hospital, Harvard Medical School, Boston, MA, USA. [10]Department of Medical Oncology, Georges François Leclerc Cancer Center-Unicancer, Dijon, France. ✉e-mail: Bertrand.routy@umontreal.ca